Liquid Fuel Fires

65

D.T. Gottuk and D.A. White

Introduction

Liquid fuel spill and pool fires represent potential hazards in many applications ranging from accidents at industrial plants using combustible liquids to arson fires with flammable fuels. A pool is characterized as a confined body of fuel that typically has a depth greater than 5 mm. A pool can result due to a liquid fuel release that collects in a low spot, such as a trench, or can exist as a result of normal storage of fuels in tanks and containers. A fuel spill is generally associated with thin fuel layers resulting from an unconfined release of fuel. The nature of a spill fire is highly variable, depending on the source of the release, surface features of the substrate (e.g., concrete, ground, water) on which the fuel is released, and the point and time of ignition. The ability to characterize fuel spills and the resulting fires in a consistent and conservative manner is required for many engineering analyses. This chapter provides an overview of the most relevant factors and methodology for evaluating a liquid fuel spill or pool fire in terms of fire growth and size.

The chapter is organized in three major sections corresponding to the three primary steps of evaluating the development of a liquid fuel spill or pool fire: (1) "Spill or Pool Size," (2) "Fire Growth," and (3) "Fire Size." The first section deals with the process of estimating the physical size of any given fuel release or pool of fuel. Both static (fixed quantity of liquid) and continuously flowing spill fires have been considered. Once a liquid fuel spill or pool has occurred, ignition of the fuel will lead to a transient fire growth period. This transient period of a liquid fuel fire is dictated by the flame spread rate across the surface of the liquid. The second section of the chapter addresses the assessment of fire growth rate by providing an overview of flame spread on liquid fuels. The third section discusses the available data and correlations that can be used to evaluate the size of the fire in terms of heat release rate and flame height.

The heat release rate of a fire is the primary parameter used in determining the impact of a fire on its surroundings. The impact of a fire is dealt with in other chapters of this handbook. The heat transfer from liquid fuel spill or pool fires is addressed by Beyler [1].

Spill or Pool Size

The first step in analyzing a liquid fuel fire is to characterize the physical dimensions of the fuel spill or pool. The area of the initial body of fuel will correlate to the size of the resulting fire. A confined fuel release or existing open container of fuel will result in a pool fire of a known area. A pool fire represents a body of fuel that is confined by physical boundaries. In other words, the walls of a room or obstructions on a floor will limit a fuel release to a smaller area than the potential

D.T. Gottuk (✉) • D.A. White
Jensen Hughes, 3610 Commerce Drive, Suite 817
Baltimore, MD 21227, USA

M. Hurley (ed.), *SFPE Handbook of Fire Protection Engineering*,
DOI 10.1007/978-1-4939-2565-0_65, © Society of Fire Protection Engineers 2016

unconfined spill area. In almost all cases, a confined fuel release will create a pool that has a greater depth than the depth of an unconfined spill. When fuel is released onto a surface, it will spread laterally based on several factors, including the initial momentum of the fluid, the fluid surface tension, and the features of the substrate onto which it spilled. Some substrate features that need to be considered are porosity of material and surface roughness. Porous materials, such as sand or even some floor coverings like carpet, can result in different spill sizes and different fuel burning rates. Surface structure can have similar effects, either by impeding liquid spread due to roughness, non-uniformity pooling, or by exaggerating liquid spread via slopes.

In general, fuel spills can be characterized as either continuously flowing or instantaneous (static). These characterizations are considered with respect to when the spill is ignited. In the case of a continuously flowing spill, ignition has occurred while the fuel is moving away from the source. For a static spill, the fuel nominally spreads to a maximum area and then is ignited, such that the flame spreads across the fuel surface. For a continuously flowing spill fire, the flame may spread across the fuel surface initially, but the flame front is ultimately controlled by the spread of the fuel over the substrate until steady-state burning conditions occur.

The area of a continuously flowing spill that is not burning will continue to increase until a physical boundary is reached or the source of the release is exhausted. A continuous spill that is burning will have a steady-state spill size based on a balance between the volumetric flow rate and the volumetric burning rate of the fuel. This concept is developed later in the section "Fire Size."

For a confined pool, the area, A, is dictated by the boundaries, and the pool depth, δ, can be simply calculated based on the volume, V, of liquid:

$$\delta = \frac{V}{A} \tag{65.1}$$

For an unconfined spill, the area has typically been determined via Equation 65.1 with an estimate of the fuel depth. In the past, engineers have conservatively estimated spill depths based on the minimum depth required to support flame spread (see "Fire Growth Rate" section). The use of a minimum depth will result in the largest possible spill area that can support a flame, therefore, the largest possible fire.

Literature results provide a basis for estimating spill depths. Table 65.1 summarizes spill depths for both noncombustible liquids and combustible fuel spill fires on unconfined surfaces. Although the table shows a range of fluid depths, the data can be simplified when considering only a range of typical hydrocarbon fuels that are commonly associated with fire scenarios, as discussed below.

The most recent work of Benfer [7] and Mealy et al. [8], systematically evaluated spill depths for a range of liquids and substrates. The average spill depth for all liquid/substrate combinations evaluated by Mealy et al. [8] was 0.72 mm, which is consistent the previously cited data and the general rule proposed in the last edition of this handbook for estimating an unknown spill fire scenario. However, it should be noted that the range of spill depths measured by Mealy et al. and Benfer was from 0.12 up to 2.9 mm depending upon the specific liquid/substrate scenario. This relatively wide range of empirical depths demonstrates the importance of understanding key variables governing fluid spread such that an appropriate spill depth is used when performing an engineering analysis. The primary two factors governing the spread of a liquid and the spill depth are the surface tension of the liquid and the surface characteristics of the substrate.

Fundamental fluid dynamics and empirical data have clearly established that spill depth is a function of the surface tension of the liquid. Figure 65.1 shows this relationship based on the experimental results for a range of liquids. As can be seen in Fig. 65.2, the surface tension of different fuels from 10 °C to 50 °C ranges from 16 to 27 dyn/cm. Water based liquids will bound most fuels of interest, as can be seen in Table 65.1 and Fig. 65.1. The surface tensions of water

Table 65.1 Summary of fixed-quantity, unconfined liquid spill data

Reference	Fuel	Quantity of fuel	Spill depth	Spill area	Surface
Chambers [2]	JP-4	4–189 L (1–50 gal)	1.1–2.9 mm	3–65 m^2	Concrete runway
Gottuk et al. [3]	Water	3.8–30 L (1–8 gal)	1.1–3.4 mm	1–11 m^2	Smooth, unfinished concrete and tile floor
Gottuk et al. [3]	6 % AFFF	3.8–19 L (1–5 gal)	0.6–1.1 mm		Smooth, unfinished concrete
Gottuk et al. [4]	JP-8	2–3 L (0.5–0.8 gal)	0.7–1.1 mm	2.1–3.1 m^2	Smooth concrete with polyuethane coating
Purtorti et al. [5]	Gasoline	0.25–1 L (0.07–0.26 gal)	0.5–0.7 mm	0.4–1.8 m^2	Wood parquet and vinyl tile
Modak [6]	#2 fuel oil	0.005–0.030 L	0.22 mm	0.0075–0.04 m^2	Both epoxy-coated concrete and steel (spill depths were the same for both surfaces and were independent of the volume of liquid spilled.)
	Lubricating oil		0.34 mm		
	Motor oil		0.75 mm		
	Hydraulic oil		0.84 mm		
Benfer [7]	3 % AFFF	0.2–450 mL	0.17–0.65 mm	0.01–1 m^2	Smooth, unfinished concrete
	6 % AFFF		0.22–0.67 mm		
	Water		0.95–2.9 mm		
	Gasoline		0.22–0.64 mm		
	Denatured alcohol		0.12–0.77 mm		
Mealy et al. [8]	All	0.25–20 L (0.07–5.2 gal)	0.72 + 0.34[a]	0.2–30 m^2	Smooth, unfinished concrete/ smooth concrete with polyurethane coating/brushed concrete/plywood/oriented strand board/vinyl tile
	3 % AFFF		0.43 + 0.15[a]		
	3 % FP Foam		0.97 + 0.53[a]		
	Lubricating Oil		1.54 + 0.55[a]		
	Gasoline		0.71 + 0.15[a]		
	Kerosene		1.01 + 0.10[a]		
	Denatured Alcohol		0.79 + 0.17[a]		
	All[b]		0.66 + 0.18[a]		Coated concrete
			0.53 + 0.08[a]		Smooth concrete (sample 1)
			0.53 + 0.20[a]		Smooth concrete (sample 2)
			0.76 + 0.26[a]		Brushed concrete
			0.63 + 0.26[a]		Vinyl flooring
			1.02 + 0.41[a]		Plywood
			1.04 + 0.51[a]		Oriented strand Board

[a]Values presented are average spill depths measured during multiple tests with one standard deviation
[b]All fuels noted for Mealy et al. reference, excluding lube oil

is 73 dyn/cm and AFFF has a value of approximately 15–16 dyn/cm at temperatures of 15–32 °C [9]. Figure 65.1 shows results for 3 % aqueous film forming foam (3 % AFFF) concentrate and a 3 % fluoro-protein foam concentrate (3 % FP) with surface tension of 17 and 27 dyn/cm, respectively.

Given that the surface tension of most fuels is relatively similar (i.e., 20–27 dyn/cm); this parameter is generally not as influential when

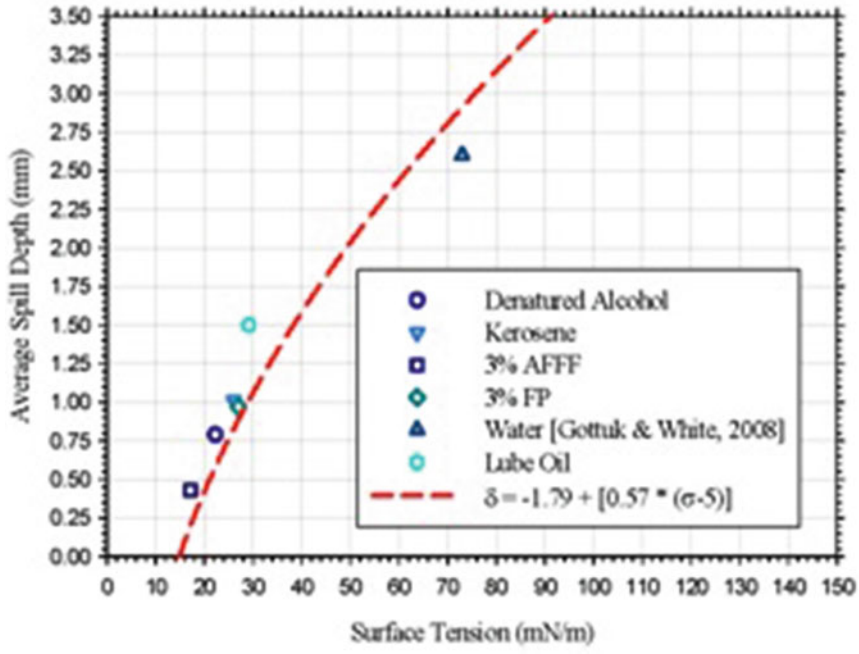

Fig. 65.1 Relationship between average spill depth and liquid surface tension [8]

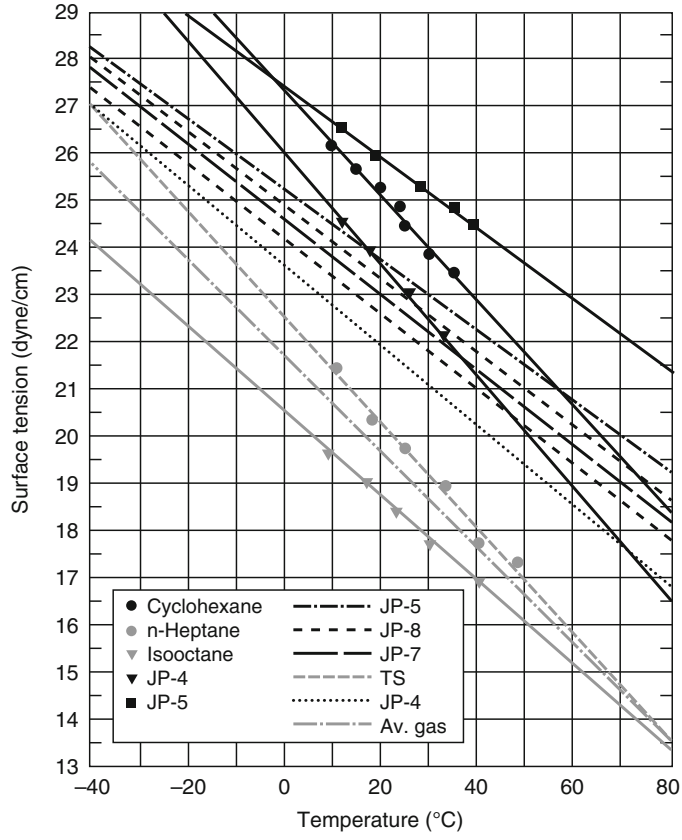

Fig. 65.2 The effect of temperature on surface tension of hydrocarbon liquids (Data taken from Moran et al. [9] and CRC [10])

considering the characteristics of a fuel spill (i.e., average depth variation of 0.71–1.01 for fuels excluding lube oil, which has a surface tension above 27) (see Fig. 65.1). The more dominant variable is the surface topography which can play a larger role in the extent of spread and the spill depth. The impact of substrate on spill depth is shown in Table 65.1. The roughness and uniformity of a substrate will dictate the speed and extent to which a liquid spreads and, thus, the equilibrium spill depth. For rougher, non-uniform surfaces, deeper equilibrium spill depths will be achieved due to the fuel being unable to spread to its full potential. Deeper spill depths result in longer burning durations with higher peak mass burning rates (i.e., larger fires). It is for this reason, from a spill dynamics standpoint, that an understanding of the surface on which a spill occurs is typically more important than understanding the fuel that was spilled.

Although from an ideal fluid dynamics point of view [8], there should be no dependence of spill depth on spill quantity, empirical data as well as transient spill models (Raj et al., 1974 and Grimaz et al., 2007) indicate that some dependence exists. These inconsistencies are an artifact of the variability in the surface characteristics that are not accounted for in the theoretical solution using ideal smooth, flat surfaces. Figure 65.3 shows the spill areas per unit volume and spill depths from spilling 0.5, 5.0, and 20 L of 3 % AFFF and 3 % FP on smooth concrete [8]. The measured area per unit volume for these scenarios consistently decreased with increasing fuel spill quantity, which is indicative of an increasing trend in spill depth. The JP-4 fuel spill data of Chambers [2] (Table 65.1) shows a similar trend for spills on a concrete runway, but with higher depths; the area per volume of fuel spilled decreased from 0.88 to 0.34 m^2/L for spills ranging from 4 to 190 L with a corresponding increase in spill depth from 1.1 to 2.9 mm. Due to limited experimental data, this data by Chambers provides the best estimate of upper limit fuel depths for large quantity spills at a time of 120 s. Spill depths of upwards of 3.4 mm were also noted for spills of water up to 30 L (where water has a surface tension of 73 dyn/cm compared to most fuels, which are below 27).

Total spill area will also be dictated by time until the liquid spread reaches the maximum area. Various spread models can be used for estimating this transient period; however, the use of idealized substrates will impact the results [8]. Based on the results from extended duration spill tests [8] with liquids (3 % AFFF, 3 % FP and gasoline) of 0.25–0.5 L spilled on smooth, impermeable surfaces (i.e., coated concrete and vinyl), the spill area was at least 90 % of the maximum spill area by 300 s. At 30 s, the spill area was approximately 50 % of the maximum steady-state area. This transient development period can have an impact on the resulting fire size

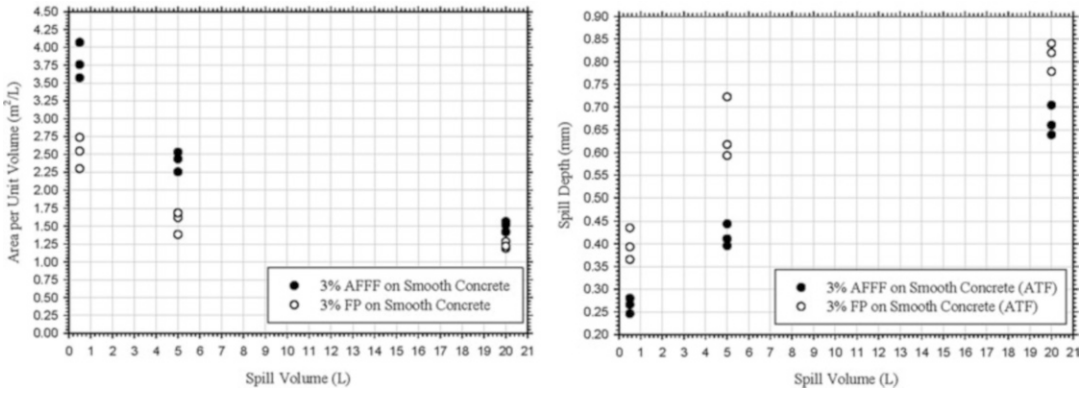

Fig. 65.3 Comparison of area per unit volume (*left*) and spill depth (*right*) to various quantity spills of 3 % AFFF and 3 % FP on smooth concrete (surface tension of 17 and 27 (dynes/cm, respectively))

based the time of ignition compared to the time to reach the maximum spill area [8].

For similar test on coated concrete, vinyl, and smooth concrete, lube oil exhibited a slightly different trend then the other liquids, reaching 75–90 % of the total spill area in the initial 30-s. This larger fraction is attributed to the high viscosity of the liquid relative to all other liquids. The high viscosity of the lube oil inhibits the spread of the liquid beyond the initial spill area.

Spills on rough/absorbent surfaces or spills involving fluids with high viscosities, generally achieve a large fraction of their spill area potential soon after being spilled. The lack of fluid spread after the initial spill can be attributed to several different factors including; the physical characteristics of the substrate impeding the movement of the fluid, the absorbency of the substrate removing liquid from the bulk flow of fluid thus reducing the spill area potential, or the internal forces within the liquid (i.e., viscosity) inhibiting the spread of the spilled volume.

As can be noted in Table 65.1, there is quite a bit of variability in spill depths for smaller quantities of fluid. The larger variability of depths for smaller spill quantities is attributed to the greater dependency on multiple variables, such as the initial spill height, surface features, and fluid properties. An example of the variability in spill depths is shown in Fig. 65.4, which presents the 6 % AFFF solution and water data of Fig. 65.1. For the water, depths varied for releases at different heights and different quantities. However, this effect was not observed for releases of the 6 % AFFF solution. Figure 65.4 also shows that similar water spills on vinyl tile floor produced the same spill depths as released on smooth concrete. Modak [6] reported that for very small spills of various oils (see Table 65.1) on steel and epoxy-coated concrete, the spill areas (and depths) were the same for both substrate materials. However, spill areas were smaller for untreated concrete due to fuel absorption into the substrate surface. This is similar to the trends observed by Mealy et al.

In summary, spill depths for liquids can vary significantly based on a number of factors ranging from the type of liquid and substrate, the volume spilled, the time frame and other spill parameters. However, as a general rule for common fuels, a spill depth of 0.7 mm can be used with reasonable confidence. Based on the work of Mealy et al. [8], the differences in calculated mass burning rates resulting from the use of an average spill depth of 0.7 mm as opposed to a substrate specific mass burning rate value were generally small and highly dependent upon the

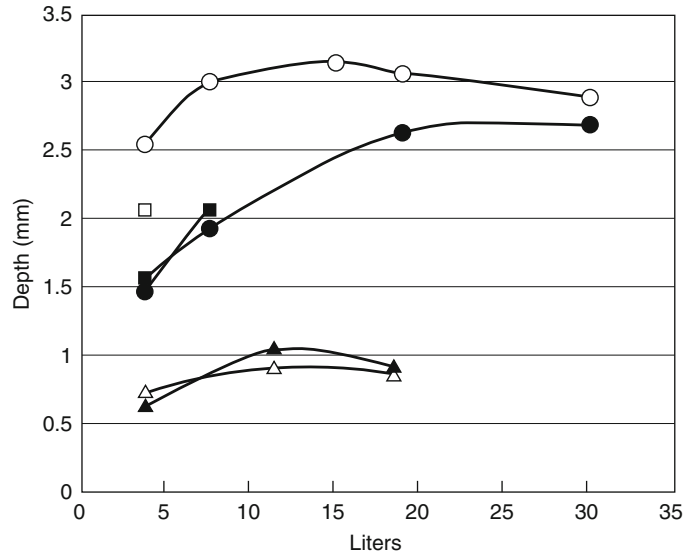

Fig. 65.4 Spill depths for 6 % AFFF solution and water releases on smooth concrete and tile floors for various fuel volumes and release heights: [3] AFFF on concrete from 0.6 m (△), AFFF on concrete from 1.0 m (▲), water on concrete from 0.6 m (○), water on concrete from 1.0 m (●), water on tile floor from 0.15 m (□), and water on tile floor from 0.9 m (■)

quantity of fuel spilled. The use of the 0.7 mm spill depth approximation as opposed to a substrate specific spill depth for spills greater than 1 L (0.26 gal), will provide baseline mass burning data that is accurate to within 10 %.

Based only on the few tests by Chambers [2] for JP-4 fuel spilled on a concrete runway, large quantities of fuel (~38 L (10 gal) and more) may result in deeper spill depths of upwards of 3 mm. This greater depth can be used as a bounding value in a fuel spill fire analysis when a longer lasting but smaller fire is worth evaluating compared to using a depth of 0.7 mm. Equation 65.4 summarize the rule of thumb for fuel depths, $\boldsymbol{\delta}$:

$$\boldsymbol{\delta = 0.7 \text{ mm for most fuels and conditions}} \tag{65.2a}$$

$$\boldsymbol{\delta = 2.9 \text{ mm for quantities of 38 L(10 gal) where analysis warrants longer duration fires}} \tag{65.2b}$$

If a more accurate estimate is needed, then Table 65.1 and reference [4] should be used to provide guidance.

It is also interesting to note that Chambers [2], Gottuk et al. [3], and Putorti et al. [5] observed increases in burning fuel spill areas after the liquid spill was ignited. Fires increased the initial fuel spill area by 22–89 % for fuel releases ranging from 2 to 190 L. The practical implication of this increase in spill area is that the fires may be substantially larger than would be predicted per the initial fuel spill areas. However, the larger area would also result in much shorter burning times before the fuel is consumed. Since the last edition of this chapter, additional work by Mealy et al. [8] showed that there was no measurable increase in burn area compared to initial spill area on non-combustible surfaces for spills up to 20 L.

Fire Growth Rate

The temperature of the spilled liquid relative to its flashpoint is the single most important factor in identifying the flame spread rate over the surface of the liquid. The flame spread rate, in turn, determines the heat release rate history of the growing fire. Other factors also affect the flame spread rate, including the depth of the spilled liquid, size of the spill, type of liquid, and the substrate.

Generally, hazard assessments involving flammable, liquid pool fires require a conservative characterization of the fire growth rate history, peak burning rate, and fire duration. The purpose of the hazard assessment often defines that only a subset of these parameters are required. Peak burning rate and maximum burning duration at the peak burning rate are typically relevant to fire effects such as fire exposure to building elements, ignition of other fuel targets, or general environmental conditions that result from the fire.

The characterization of the spill or pool fire heat release rate history from ignition to peak burning rate (full involvement of pool fuel surface area) is important when dealing with time-related concerns or events. Examples of time-dependent concerns include egress or life safety conditions, activation of detection or suppression systems, spread of fire to other fuel packages, or failure of building elements. Presuming that one is interested in the pool fire heat release rate growth history, this can be defined as the integration of the flame spread rate for the particular geometry in question (e.g., circular for unconfined pools, rectangular for trenches) multiplied by the burning rate per unit surface area for the given liquid. Estimating the flame spread rate over the surface of the flammable/combustible liquid spill becomes critical in characterizing the fire growth history.

Most ignitions of flammable liquid fuels result in flame spread that can be characterized by one of two major flame spread mechanisms for liquid fuels: liquid phase-controlled flame spread or gas phase-controlled flame spread. Flame spread rates for these two regimes can be grossly benchmarked: 1–12 cm/s for liquid phase-controlled flame spread and 130–220 cm/s for gas phase-controlled flame spread. A third regime for flammable liquid spills on porous surfaces can be defined where flame spread rates are measured in terms of cm/min. For some hazard analyses, identifying the appropriate flame spread region may sufficiently characterize the flame spread rate in a conservative fashion. The primary driver of the flame spread regime is the temperature of the spilled liquid relative to its flashpoint.

Basic Theory of Flame Spread on Liquids

Flame spread on liquid fuels has been widely studied in small-scale experiments and theoretical studies [11–29]. The flame spread rates are known to be dependent on fuel temperature and fuel flashpoint. Below the flashpoint temperature, the flame spreads by way of surface tension-induced flow of hot fuel ahead of the advancing flame. Above the flashpoint, the flame spread is by way of gas phase spread, which can be as rapid as 2 m/s. The majority of liquid flame spread studies have been limited to pure fuels, and most of the studies have used alcohol fuels in trays less than 10 cm wide. The majority of liquid flame spread studies have been focused on pure fuels with heavy emphasis on alcohol fuels in trays less than 10 cm wide. This chapter includes empirical data from nonpure hydrocarbon fuels [30] as well as data from large-scale studies [8, 31].

Flame Spread Regimes Several flame spread regimes have been identified in the literature. These flame spread regimes are most notably a function of the liquid temperature. The dependence of flame spread rates on liquid temperature has been studied by a number of investigators [11–27]. The most extensive work has been done with narrow pans of alcohol fuels with fuel depths of 2–5 mm. These investigations indicate that the flame spread velocity is a strong function of fuel temperature, even when the fuel temperature is well below the flashpoint. Figure 65.5 shows the extensive work that Akita [14] conducted using methanol in a 2.6-cm-wide pan. Akita observed a number of different flame spread regimes. Above the flashpoint, spread was via the gas phase. Below the flashpoint, he

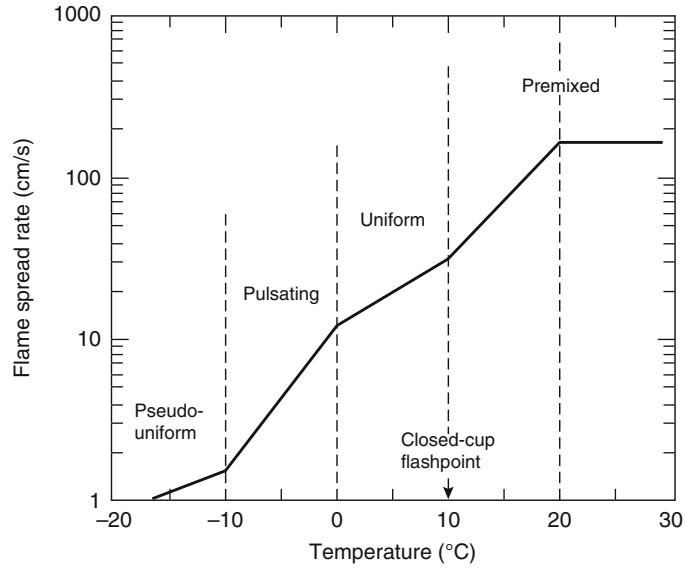

Fig. 65.5 Flame spread rate on 1-cm-deep methanol as a function of fuel temperature in a 2.6-cm-wide pan [14]

observed regions of uniform, pulsating, and pseudo-uniform spread. The mechanistic explanations for these phenomena below the flashpoint are not widely agreed upon. A more detailed discussion of flame spread regimes and their mechanisms can be found in the review article by Ross [32].

Semilog plots of flame spread rate as a function of liquid temperature have a characteristic shape with three regions: the liquid-controlled region, the gas phase–controlled region, and the asymptotic gas phase-controlled region. The slopes of the curve are different in each of these regions, and these differing slopes serve to define the regions. The transition from liquid to gas phase–controlled burning occurs at a temperature T_{go}; the transition from gas phase control to asymptotic gas phase spread occurs at a temperature T_{gm}. Figure 65.6 graphically portrays these temperatures with respect to flame spread rates. Figure 65.6 is intended as a conceptual depiction and the omission of units on the axes is intentional.

Figure 65.6 is conceptually the same as a figure first described by Glassman and Hansel [33]. In their paper, they identified the temperature at which gas phase-controlled flame spread begins as the firepoint of the liquid; they also identified the temperature at which the maximum flame spread rate occurs as the stoichiometric temperature (the liquid temperature at which the vapor concentration at the surface is stoichiometric). While this interpretation is consistent with the interpretation of data for multicomponent fuels, in light of Glassman and Dryer [19], it is not practical to define a firepoint temperature for a multicomponent fuel. The difficulties are due to the need to model evaporation of many high-volatility components in a multicomponent fuel during the open heating that is required in the determination of a firepoint. Determination of the firepoint of a multicomponent fuel would require closed-cup heating of a fuel to a test temperature, exposing the liquid surface, and applying an ignition source. If the fire does not continue, the test temperature is below the firepoint. Additional temperature tests would be required until the firepoint temperature is bracketed to the desired accuracy. This process is not practical. Similarly, for a multicomponent fuel it is not always practical to define the stoichiometric temperature, since determination of the vapor pressure of each component is, at the least, tedious and often impossible. Thus, while Glassman and Hansel's definitions are not easily generalized to multicomponent fuels, their pure fuel concepts can still provide guidance and

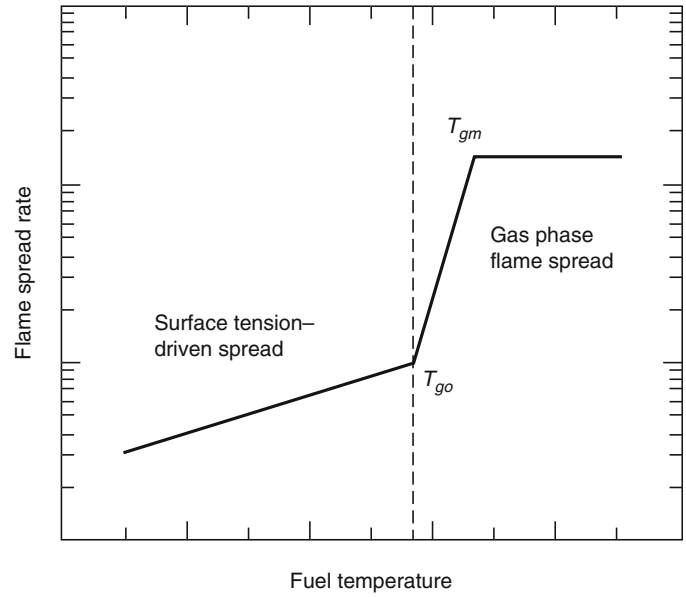

Fig. 65.6 Graphic representation of the definitions of T_{go} and T_{gm}

motivation for the interpretation of multicomponent liquid fuel flame spread results.

Pool Dimensions The physical dimensions of a liquid fuel spill or pool influence the flame spread rate, assuming an ignition source is present. The primary factors of importance are pool depth and characteristic width of the pool, as discussed below.

Pool dimensions, including fuel depth, have no effect on the flame spread rate for situations where the flame spread mechanism is considered gas phase-controlled. However, the depth of a flammable liquid does have a significant impact on the flame spread rate for liquid phase-controlled burning. In general, the average flame spread velocity for liquid phase-controlled spread increases with fuel depth, which is primarily governed by whether the fuel release is confined or unconfined.

Scientific study of liquid flame spread can be traced back as far as the 1930s [11]. Most of the early work was done on relatively small-scale test setups, much using pans only 1–6 cm wide with alcohol fuels at depths of 2–5 mm [12–14]. Work by Mackinven, Hansel, and Glassman [15] at Princeton is especially relevant here because it involved extensive experiments with decane, a pure fuel with similar characteristics to aviation fuels and other low-flashpoint multicomponent hydrocarbon fuels that are common to fire hazard assessments. The Princeton research documented the effects of pan width and fuel thickness on observed flame spread rates [15].

Several investigators have performed experiments to characterize the impact of fuel depth on liquid-controlled flame spread. Mackinven et al. [15] demonstrated the systematic variation of flame spread rates with fuel depth. They investigated decane fuel depths from 1 mm to 2 cm and found the flame spread rate to increase with fuel depth as shown in Fig. 65.7. This increase can be attributed to the retarding effect of small fuel depths on liquid recirculation flows that cause flame spread. Calculations by Torrance [16, 17] are in excellent agreement with Mackinven et al.'s experimental data shown in Fig. 65.7. These calculations indicate that decane flame spread rates increase with pool depth up to 3 cm, with greater fuel depths beyond this no longer increasing the flame spread rate. Of course, fuel depths for unconfined fuel spills will always be far less than 3 cm. Investigations by Mackinven et al. [15] as well as Burgoyne and Roberts

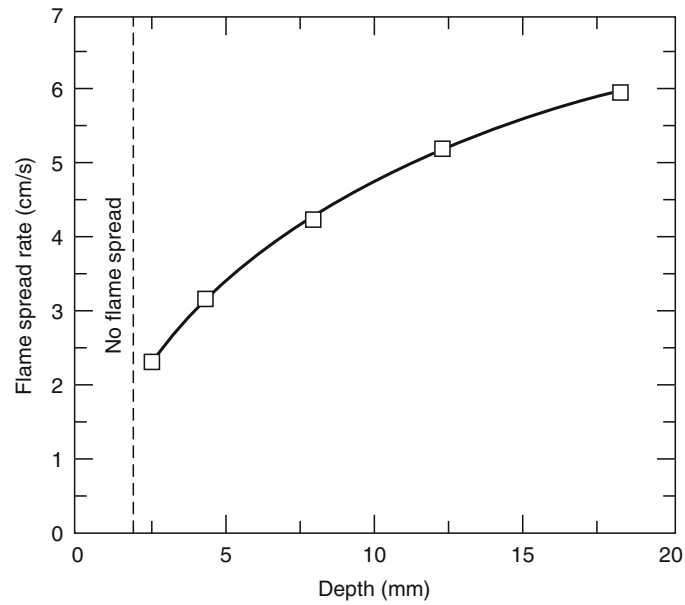

Fig. 65.7 Flame spread rate on decane as a function of fuel depth [15]

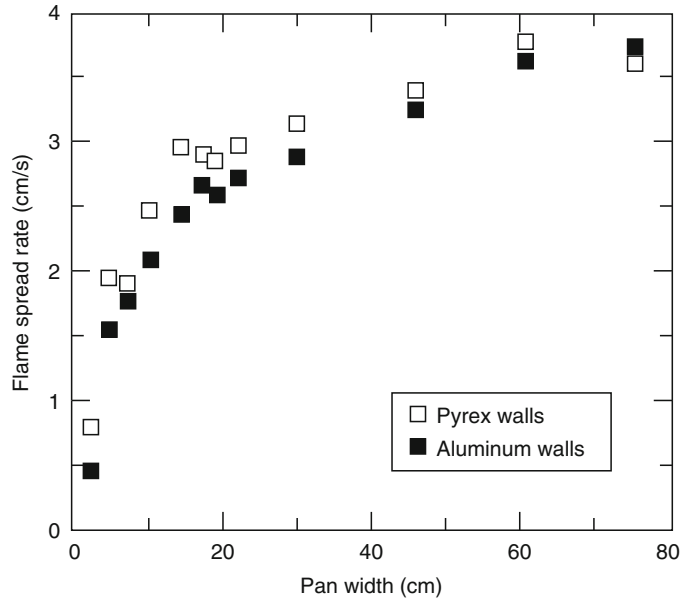

Fig. 65.8 Flame spread rate on decane as a function of pan width [15]

[12, 13] indicate that flames do not spread away from the ignition source in liquid pools at or less than 1.5 mm deep. More recent work by Burelbach, Epstein, and Plys [34] demonstrated that the limiting fuel thickness for flame spread was 2.0 mm for decane and 2.3 mm for dodecane. Minimum fuel depths for flame spread are for the liquid-controlled spread regime. There is no evidence for fuel depth or pan width effects on gas phase flame spread [12, 14, 18, 20, 23, 25].

Mackinven et al. [15] found that for pan widths up to 20 cm the flame spread rates on decane are a strong function of pan width. At pan widths from 20 to 80 cm, the maximum width they studied, they observed only slight increases in flame spread rate. Their results are shown in Fig. 65.8. Both aluminum and glass pan walls were used. The small differences between these two wall materials may be attributed to heat conduction effects; however, the major influence at pan widths less than 20 cm is independent of wall material and has been attributed to a momentum reduction associated with viscous drag on the walls. The relative independence of pan width above 20 cm indicates that flame radiation is not a pivotal mechanism in determining liquid phase-controlled flame spread. The results were confirmed by Mackinven et al. by shielding the liquid ahead of the flame from flame radiation during flame spread experiments (20- to 80-cm-wide pans). They observed modest changes in flame spread rates between the shielded and unshielded experiments.

Temperature Effects The work of Burgoyne and Roberts [12] showed that at small pan widths the temperature dependence of the flame spread rate is a function of the pan width as shown in Fig. 65.9. Unfortunately, their work extends only from 2.5 to 6.3 cm widths. The dependence on pan width disappears above 41 °C, the flashpoint of isopentanol. The work of Mackinven et al. [15] using varying pan widths (see Fig. 65.8) with decane 21 °C below the closed-cup flashpoint (44 °C) as well as work by Burgoyne and Roberts [12] indicates that pan width ceases to have an impact on the temperature dependence of the flame spread rate at pan widths greater than 20 cm.

Flame spread experiments above the flashpoint indicate that flame spread is via the gas phase. The flame spread rate increases rapidly from the flashpoint to the liquid temperature at which a stoichiometric fuel-air mixture exists above the liquid surface. Above this temperature, the flame spread rate is no longer temperature

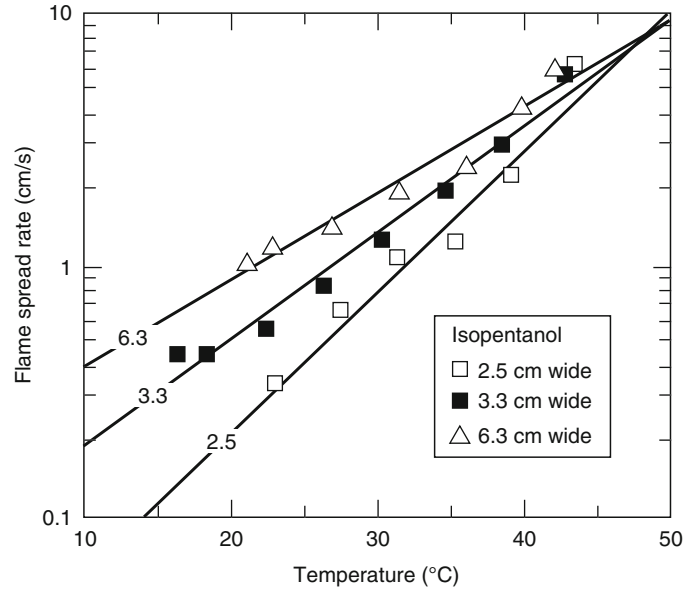

Fig. 65.9 Effect of pan width on the temperature dependence of flame spread rate on isopentanol [12]

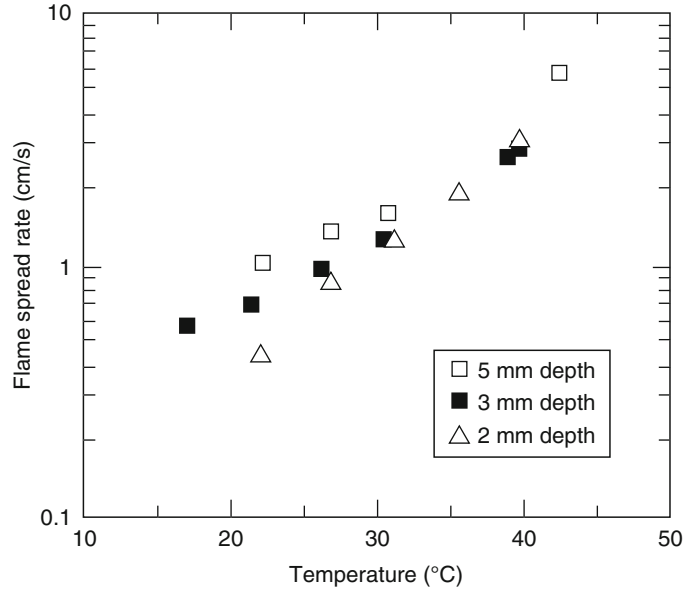

Fig. 65.10 Effect of fuel depth on the temperature dependence of flame spread rate on isopentanol [12]

dependent. The flame spread velocities measured by Burgoyne and Roberts [12], Akita [14], Nakakuki [20], and Hirano et al. [25] in this temperature region are from 1.3 to 2.2 m/s depending on the fuel. These velocities are similar to flame spread rates measured in stratified fuel-air mixtures found near ceilings of mine tunnels [35–37].

The work of Burgoyne and Roberts also indicates that the temperature dependence of the flame spread rate is a function of the fuel depth [12]. They investigated isopentanol at fuel depths of 2–5 mm and their results, shown in Fig. 65.10, indicate that variations in flame spread rate with fuel temperature below the flashpoint (41 °C) are lessened by increasing fuel depth.

Empirical Data

An overview of the experimental results for flame spread velocities follows, including alcohol fuels, multicomponent hydrocarbon fuels, and blends of multicomponent hydrocarbon fuels. Although the bulk of the data is for laboratory-scale pools, there is limited data for large-scale pools of hydrocarbon fuels as well as some data for large-scale spills of jet fuel (hydrocarbon).

White, Beyler, Fulper, and Leonard [30] measured flame spread rates for aviation fuels, mixtures of these multicomponent hydrocarbon fuels, as well as 1-pentanol (alcohol). These measurements were made over a range of fuel temperatures in a pan 20 cm wide by 163 cm long. The results for pure JP-5 and JP-8 are shown in Figs. 65.11 and 65.12. The flame spread rates range from 3 to 140 cm/s over a temperature range of 10–90 °C. The solid symbols indicate liquid-controlled flame spread and the open symbols indicate gas phase flame spread. JP-5 is a high-flashpoint kerosene used by the U.S. Navy that has a specified minimum flashpoint of 60 °C [38]. JP-8 is a newer U.S. Air Force fuel, very similar to commercial Jet A-1, that is a kerosene with a lower specified minimum flashpoint of 38 °C [39]. The flame spread rates in the liquid-controlled regime for JP-8 are 0.5–2 cm/s greater than for JP-5. At temperatures approximately 12–20 °C above the closed-cup flashpoint, flame spread rates increase very rapidly to over 100 cm/s. The major difference in flame spread characteristics of JP-5 and JP-8 is the temperature at which the flame spread rate rapidly increases: 68 °C for JP-5 and 58 °C for JP-8.

Figure 65.12 shows several data points where the application of the ignition source was systematically varied from 3 to 460 s in the most sensitive temperature region (the transition between liquid-controlled and gas phase–controlled flame spread). At higher and lower temperatures such ignition delays have little or no effect on the observed flame spread rate. Assuming that the flame spread rate is a function of the liquid temperature relative to the flashpoint temperature, the results are consistent with an increase in the flashpoint of approximately 10 °C during the 3–460 s between fuel discharge and ignition. No systematic study of flashpoint variations with time for multicomponent fuels appears elsewhere in the literature.

The flame spread results for JP-5 and JP-8 indicate that the single most important determinant of flame spread is the initial temperature of the liquid prior to ignition relative to the fuel's

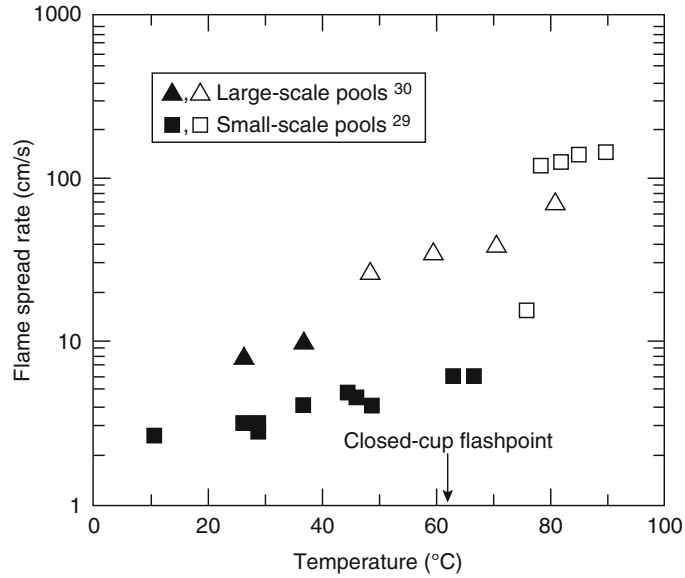

Fig. 65.11 Flame spread rate for JP-5 as a function of temperature. *Solid symbols* denote liquid-controlled flame spread and *open symbols* denote gas phase flame spread for small-scale data only

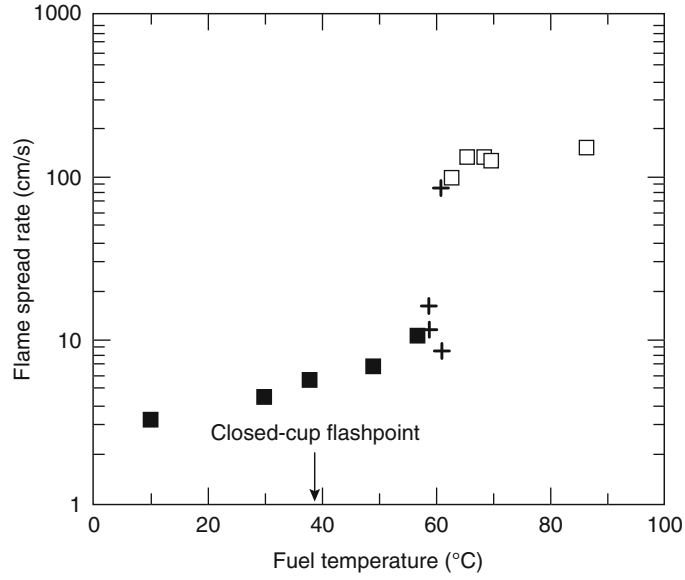

Fig. 65.12 Flame spread rate for JP-8 as a function of temperature. *Solid symbols* denote liquid-controlled flame spread and *open symbols* denote gas phase flame spread; + indicates variable times to ignition of 3, 160, 240, and 460 s. The normal time to ignition is 35 s. Longer ignition times reduce the flame spread rate [30]

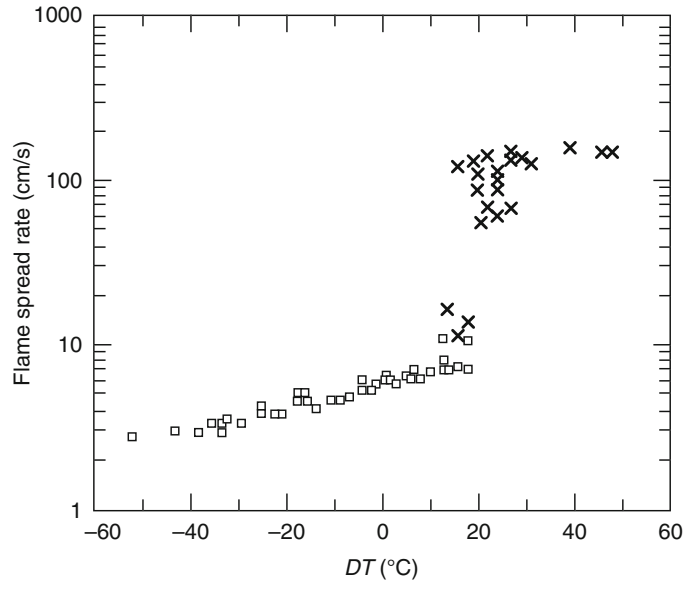

Fig. 65.13 Flame spread rate for all JP fuels as a function of $DT(T_{fl} - T_l)$ [30]

flashpoint. Hillstrom [18] also observed this correlation and found that plotting the flame spread rate as a function of the temperature difference between the closed-cup flashpoint, T_{fl}, and the liquid fuel temperature, T_l, correlated data for a number of hydrocarbon fuels. Figure 65.13 shows flame spread rate data for pure JP-5, pure JP-8, and mixtures of the two fuels plotted as a function of $DT(T_{fl} - T_l)$. In Fig. 65.13 square symbols represent liquid-controlled flame spread and the *X* symbols indicate gas phase flame spread. The treatment of the data effectively correlates all of the jet fuel data over a range of *DT* from −50 °C to +50 °C. This representation of the data clearly shows the importance of *DT* $(T_{fl} - T_l)$ in determining flame spread rate.

Figure 65.13 also shows excellent consistency in the transition from liquid-controlled flame spread to gas phase spread at $DT = 18$ °C.

Leonard et al. [31] performed large-scale flame spread experiments as part of an effort to evaluate the fire hazards of mixed jet fuels on aircraft carrier flight decks. The experiments, which evaluated pure JP-5, pure JP-8, and mixtures of these two jet fuels, were carried out in a large-scale pan 1.52 m in width by 12.2 m in length. The Leonard et al. experiments are the largest pool fire flame spread experiments reported in the literature. The jet fuels were evaluated over a range of temperatures by introducing heated fuel into the large pan, which was also temperature controlled by circulation of water through chambers on the underside of the pan bottom. The results for JP-5 are presented in Fig. 65.11. The results for JP-8 are illustrated in Fig. 65.14.

The large-scale results can easily be compared with small-scale results in both Figs. 65.11 and 65.14. This comparison yields identical qualitative results. The flame spread rates for the large-scale tests are notably higher for both the JP-5 and JP-8 liquid-controlled flame spread tests. Data for the JP-8 tests indicate that the liquid-controlled flame spread rate is 10–11.6 cm/s whereas the JP-5 tests show 8.2–10 cm/s in this regime. As with the small-scale tests, there is approximately 1.5–1.8 cm/s difference between the two jet fuels, with the JP-8 fuel slightly faster. The transition to gas phase flame spread appears to occur at a lower temperature for both fuels. Similar gas phase flame spread velocities are obtained between small- and large-scale tests. The disparity between the small- and large-scale tests for these two fuels cannot be attributed to a single factor. It is speculated that the difference in flame spread behavior of the two experimental data sets may be due, in part, to width effects and flame radiation effects. Further work is necessary to identify the specific mechanisms responsible for this observed difference.

A recent set of experiments evaluating aircraft hangar fire detection technologies [8] included large-scale jet fuel spill fires. The work of Hill, Scheffey, Walker, and Williams [8] evaluating alternative fire protection methods for U.S. Air Force aircraft hangars represents the largest spill fires evaluated in the literature for flame spread. A volume of 114 L (30 gal) of JP-8 was spilled on a concrete pad. The main focus of this research was fire suppression systems, and an important aspect evaluated was the impact of various suppression systems on the flame spread rate after system activation. Experiments measured the flame spread rate over the large

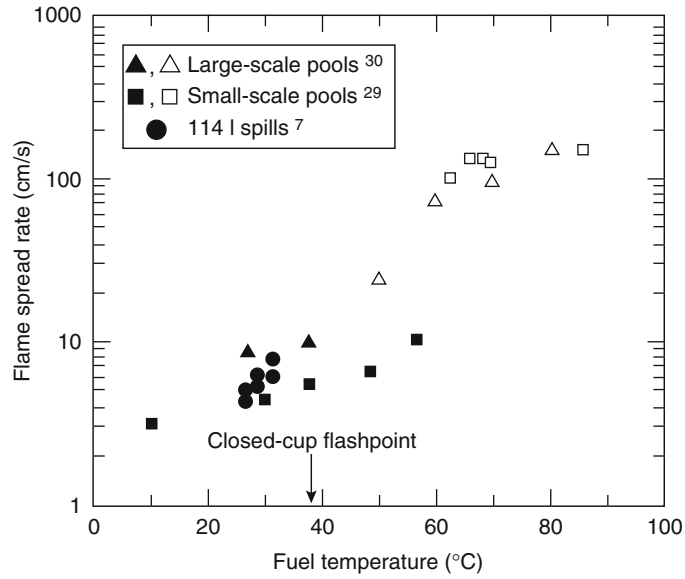

Fig. 65.14 Flame spread rate for JP-8 as a function of temperature. *Solid symbols* denote liquid-controlled flame spread and *open symbols* denote gas phase flame spread

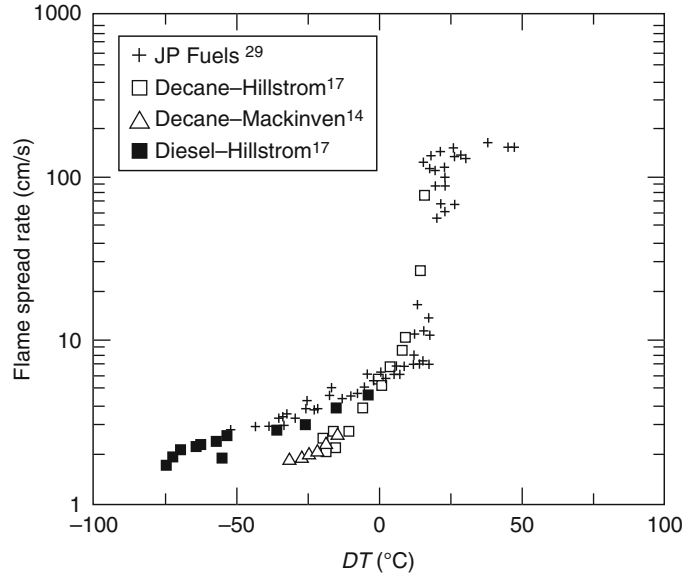

Fig. 65.15 Comparison of JP fuel data with other hydrocarbon flame spread data from the literature

spill area, which covered approximately 30 m^2 at the time of ignition, both before and after operation of the suppression system. The full free-burn spill size was on the order of 37 m^2 with time for complete burnout at roughly 2 min. Measured flame spread rates for the JP-8 spills prior to suppression system activation have been identified in Fig. 65.14. The temperature of the JP-8 fuel was approximately 25 °C ± 2 °C. These flame spread rates fall close to the data points from the small-scale tests. The Hill et al. data points show a 1.5–3.5 cm/s increase over the small-scale data for the liquid-controlled flame spread results. The large-scale spill data show higher flame spread rates in comparison to the small-scale pool experiment data.

Although there are depth issues associated with the comparison of pool experiments to spill experiments, the trend appears to be that larger-scale flame spread experiments yield higher flame spread rates for the liquid-controlled flame spread regime with a transition to gas phase spread occurring at a lower temperature than observed in the small-scale pool experiments. While these differences may not be fully explainable, it is important to note that irrespective of the experiment scale, peak flame spread rates for the liquid-controlled flame spread regime are approximately 10 cm/s for JP-5 and 12 cm/s for JP-8. Furthermore, although the transition to gas phase spread seems to occur at a lower temperature, the maximum gas phase flame spread rates are maintained in the 120–200 cm/s range for both JP-5 and JP-8. Support for using a maximum flame spread velocity of 10 cm/s for liquid-controlled flame spread over hydrocarbon fuels can be drawn from Fig. 65.15, which shows a comparison of the jet fuel data from White et al. [30] and other hydrocarbon data from the literature. The results of the jet fuels were consistent with those of Hillstrom [18] and Mackinven et al., [15], which show a very modest variation in flame spread rate below the flashpoint temperature. Figure 65.15 shows a comparison between the jet fuel data of White et al., [30], the decane data from Hillstrom [18], the diesel fuel data from Hillstrom [18], and the decane data from Mackinven et al. [15]. The decane results show a rise in the flame spread rate at a smaller value of *DT* than for the JP fuels. Also, below the closed-cup flashpoint, the decane shows lower flame spread rates. This variation may be due to the effect of using a water substrate in the decane tests rather than steel as used in the jet fuel work. All the data in Fig. 65.15 were collected in 20-cm-wide pans.

Empirical data for flame spread over alcohol pools consist of small-scale test data. White et al. [30] performed the largest experiments, utilizing a 20-cm-wide pan evaluating 1-pentanol as part of their study. Results from these 1-pentanol flame spread tests, illustrated in Fig. 65.16, were performed to assess the effect of fuel type on flame spread for an alcohol fuel that had a similar flashpoint to the jet fuels primarily under study in this specific piece of work. Pentanol was chosen, in part, due to the previous pentanol flame spread work performed by Burgoyne and Roberts [12].

Liquid-controlled flows were observed at temperatures less than 52 °C. The change from liquid-controlled flame spread to gas phase flame spread occurred at approximately 4 °C above the closed-cup flashpoint. Figure 65.16 illustrates a comparison of the 1-pentanol results from White et al. [30] with the alcohol data from Burgoyne and Roberts [12]. The 1-pentanol results take on the same characteristic dependence on *DT*, with the Burgoyne and Roberts data showing rapid rise in the flame spread rate at somewhat lower values of *DT* than the 1-pentanol data. The slope difference between the Burgoyne and Roberts data and the 1-pentanol data for the liquid-controlled flame spread regime can be attributed to the effect of pan width on the temperature dependence of flame spread rate in this regime. It is very interesting to note that in Fig. 65.16 the data for alcohol flame spread are similar to the hydrocarbon data with respect to the maximum of 10 cm/s liquid-controlled for flame spread rates with the gas phase flame spread rates falling between 150 and 200 cm/s.

Table 65.2, reproduced from White et al. [30] shows the closed-cup flashpoint, T_{fl}, the transition from liquid to gas phase-controlled burning, T_{go}, and the transition from gas phase control to asymptotic gas phase spread, T_{gm}, for the small-scale jet fuel data, the 1-pentanol data, and the decane data from Hillstrom [18]. The difference $T_{go} - T_{fl}$ averages 15 °C for the hydrocarbon fuels. The difference $T_{gm} - T_{go}$ averages 6 °C and the overall difference $T_{gm} - T_{fl}$ averages 21 °C. These results may be expected to represent general properties for small hydrocarbon pools but should not be used for alcohol fuels.

Glassman and Dryer [19] have pointed out some discrepancies in the measurement of flashpoints and firepoints of alcohols versus hydrocarbons and the relevance of flashpoints to the hazards of liquid fuels. Although each of the standard flashpoint/firepoint testing methods has its own difficulties, it is clear from the work

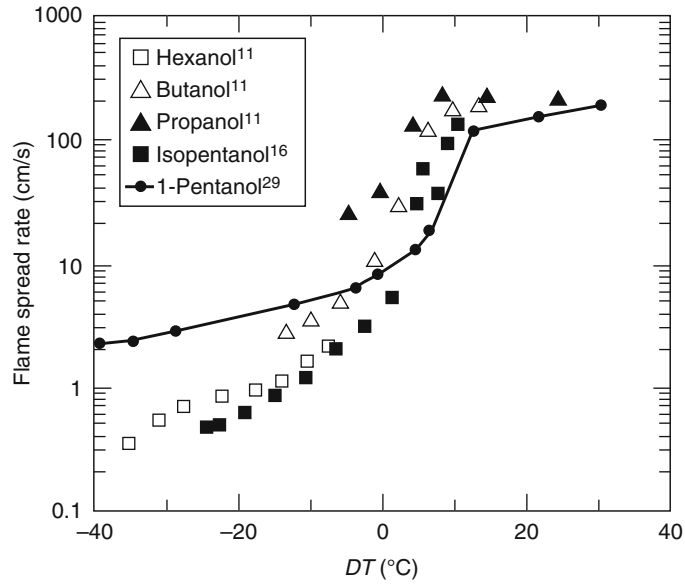

Fig. 65.16 Comparison of the 1-pentanol data with the alcohol (Data of Burgoyne and Roberts [12])

Table 65.2 Critical temperatures (°C) for flame spread [30]

Fuel	T_{fl}	T_{go}	$(T_{go} - T_{fl})$	T_{gm}	$(T_{gm} - T_{go})$	$(T_{gm} - T_{fl})$
JP-8	39	57	18	62	5	23
25/75 JP-8/5	42	60	18	66	6	24
50/50 JP-8/5	48	65	17	72	7	24
75/25 JP-8/5	54	68	14	74	6	20
JP-5	63	76	13	79	3	16
Decane [5]	44	56	12	62	6	18
Average 1–6	—	—	15	—	6	21
1-Pentanol	48	52	4	62	10	14

of Glassman and Dryer that none of the standard flashpoint testing methods correlate with the onset of gas phase flame spread for all fuels. Glassman and Dryer point out major differences between alcohol and hydrocarbon flashpoints and point to the large quenching diameter for these two classes of fuels. Based on Glassman and Dryer's observations, transition to gas phase flame spread would be expected at temperatures near the closed-cup flashpoint for alcohol fuels, as observed for the 1-pentanol test results.

However, there are differences in $T_{go} - T_{fl}$ between jet fuels and decane. The more volatile aviation fuels are characterized by $T_{go} - T_{fl} \sim 18\ ^\circ C$ while decane and JP-5 are characterized by $T_{go} - T_{fl} \sim 12\ ^\circ C$. This 6 °C difference may be due to the loss of light ends from the more volatile hydrocarbon mixtures and is consistent with the variations in flame spread rate with ignition time delay represented in Fig. 65.12. White et al. point out that it appears that the actual flashpoint of the JP-8 may have increased by approximately 6 °C during the discharge and ignition delay period. While this deduction seems reasonable, a more systematic study of this issue is warranted. The important consideration for hazard analyses is that multicomponent hydrocarbon fuels can incur a reduction in effective flashpoint depending on the volatility of the fuel and the time period between the fuel release and ignition. The conservative approach would be to assume instantaneous ignition of the released fuel.

Fuel-soaked beds of porous media (e.g., small beads of glass or metal) have been used in flame spread experiments to simulate a fuel spill onto a porous surface. Flame spread over porous media generally occurs at rates on the order of 1–8 cm/min, which is similar to measures of flame spread over the surface of relatively thick solids. Takeno and Hirano [40] have experimentally evaluated several parameters important to characterizing the flame spread rate over porous media soaked with fuel. Figure 65.17 represents the results from their study. Table 65.3 identifies the conditions of each experiment portrayed in Fig. 65.17.

These tests used a steel tray 3.5 cm wide and 60 cm long that was filled with either glass or lead beads. Four observations can be made from these data: (1) the flame spread velocity increases slightly as the diameter of the beads, d, increases and there appears to be little dependence on the liquid viscocity (see Fig. 65.17, conditions A, B, C) for 90 % by volume of decane and 10 % hexane; (2) the flame spread for pure decane is a function of the bead diameter and the viscosity (conditions E, F, G, H) with the flame spread velocity decreasing as d increases for smaller values of d, reaching a minimum flame spread rate at approximately $d = 0.25$ cm, from which point the flame spread velocity increases with d, and fuel viscosity effects are more pronounced with flame spread rate decreasing as the viscosity of the fuel increases; (3) for situations where the liquid level is below the top surface of the bead bed (conditions J, K), flame spread velocities are reduced and depend little on bead diameter or fuel viscosity; (4) when the glass beads are replaced with lead beads (conditions D, I, L), similar variations are observed as with the glass beads; however, the flame spread rates are reduced by approximately 10 %. In general,

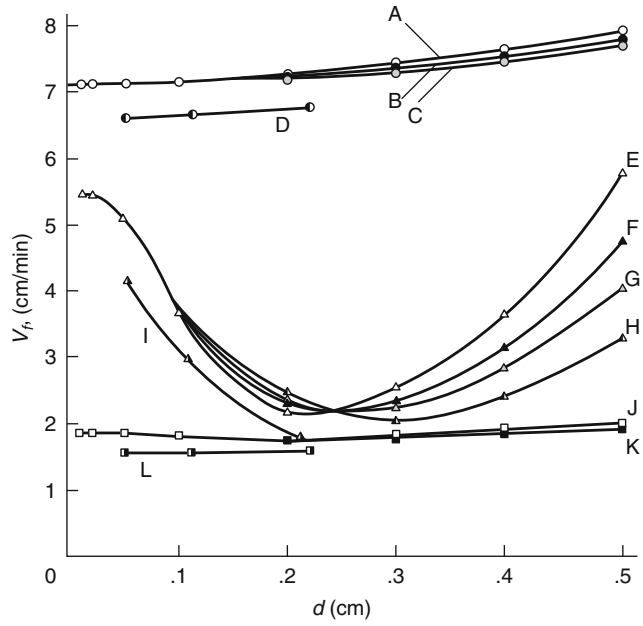

Fig. 65.17 Variations of flame spread rate with bead diameter [40]. Table 65.3 lists conditions

the flame spread rates for pure decane ranged from 2 to 6 cm/min whereas the mixtures of 90 % decane/10 % hexane spanned 7–8 cm/min.

Ishida [41] has also investigated fire growth on fuel-soaked ground with a rectangular pan using central ignition. The shallow square steel tray measured 50 · 50 · 2 cm deep. The tray was filled with glass beads. Radial flame spread rates were measured for decane fuel over varying bead diameters. Figure 65.18, which reproduces Ishida's results, demonstrates that the average flame spread velocity decreases as the bead diameter increases. It is also interesting to note that the flame spread rate accelerates as the fire size increases. The average flame spread rate over the duration from a 2 cm flame diameter to a 30 cm diameter ranges from 6 to 10 cm/min for the bead diameters investigated.

Using Flame Spread Velocities to Characterize the Rate of Involvement of a Pool or Spill

Characterizing the fire growth rate history of a fuel release fire is dependent on describing the time-dependent history of the area involved with fire. The flame spread rate must be placed in the context of the fuel release geometry as well as the location of the ignition point. Thus, the geometry of the released fuel and the relative location of the ignition source define the framework for characterizing the area of involvement.

An example for a circular pool of fuel follows. A circular pool with the ignition source in the center yields the most rapid involvement of the entire fuel release. Assuming that uniform spread occurs, a circular fire will develop and the area of the pool involved will be a function of the fire radius:

$$A_{\text{fire}} = \pi r^2 \tag{65.3}$$

where A_{fire} is the area of the fire in m^2 and r is the radius of the fire in m at any given time, t (s). Assuming a constant flame spread velocity, the radius of the burning area can be defined as

$$r = vt \tag{65.4}$$

where v is the flame spread velocity in m/s. Substituting Equation 65.4 into Equation 65.3:

$$A = \pi v^2 t^2 \tag{65.5}$$

Table 65.3 Experimental conditions of fuel-soaked beds presented in Fig. 65.17

	Combustible liquid	Viscosity μ (cp)	Material of beads	Initial liquid level y_s (cm)	Symbol
A	90 % decane + 10 % hexane	0.846 (normal)	Glass	0.0	○
B	90 % decane + 10 % hexane	2.617	Glass	0.0	●
C	90 % decane + 10 % hexane	4.552	Glass	0.0	○
D	90 % decane + 10 % hexane	0.846	Lead	0.0	◐
E	Pure decane	0.846	Glass	0.0	△
F	Pure decane	2.617	Glass	0.0	▲
G	Pure decane	4.552	Glass	0.0	△
H	Pure decane	6.872	Glass	0.0	△
I	Pure decane	0.846	Lead	0.0	▲
J	Pure decane	0.846	Glass	–0.5	□
K	Pure decane	4.552	Glass	–0.5	■
L	Pure decane	0.846	Lead	–0.5	◨

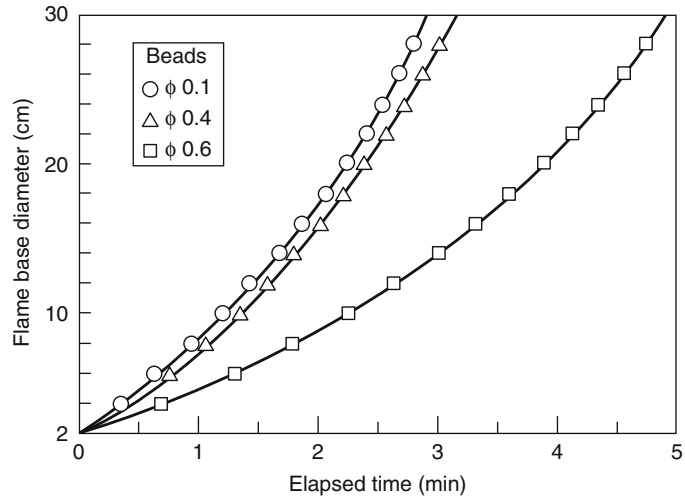

Fig. 65.18 Diameter of flame pillar base as a function of elapsed time [41]

In this manner, Equation 65.5 can be used to identify the area of the spill involved at any time subsequent to the ignition. Assuming that the mass burning rate per unit area is at a constant value $\dot{m}'' = \dot{m}''_{\max}$ and does not change as a function of time, a t^2 fire develops. Of course the time limit is defined when the fire involves the maximum area of the spill and this limit can be defined as follows:

$$t_{A,\max} = \frac{r_{A,\max}}{v} \tag{65.6}$$

where $t_{A,\max}$ is the time the entire pool surface becomes involved with fire, and $r_{A,\max}$ is the maximum radius of the fuel release.

A similar approach can be applied to a rectangular trench. Assuming an ignition source at one end of the trench, an alternative example can be developed. The trench geometry area is defined as

$$A = wl \tag{65.7}$$

where w is the width of the trench in m and l is the length of the trench involved with fire in m. Assuming w is small compared to l and that the ignition source at one end of the trench spans the width of the trench and that the flame spread rate is constant, the length of trench involved is

$$l = vt \tag{65.8}$$

Substituting Equation 65.8 into Equation 65.7 yields the time-dependent area of the trench involved:

$$A = wvt \tag{65.9}$$

In this manner, Equation 65.9 can be used to identify the area of the trench involved at any time subsequent to the ignition at one end. Assuming that the mass burning rate per unit area is at a constant value $\left(\dot{m}'' = \dot{m}''_{\max}\right)$ and does not change as a function of time, a t^1 fire develops. Of course the time limit is defined when the fire involves the maximum area of the trench and this limit can be defined as follows:

$$t_{A,\max} = \frac{l_{\max}}{v} \tag{65.10}$$

where $l_{\max}$ is the maximum length of the trench.

This type of approach can be used for other fuel release configurations and ignition source locations. The heat release rate is then the area of the fuel release involved multiplied by the burning rate per unit area as well as the heat of combustion. This relationship is explained in more detail in the following section.

Fire Size

The fire size is primarily characterized by the heat release rate and the flame height. The heat release rate, $\dot{Q}$, is calculated as

$$\dot{Q} = \dot{m} \cdot \Delta h_c \tag{65.11}$$

where $\dot{m}$ is the mass burning rate of the fuel and Δh_c is the fuel heat of combustion. The fuel mass burning rate can be calculated via Equation 65.12 or 65.13 as follows:

$$\dot{m} = A \cdot \dot{m}'' \tag{65.12}$$

where A is the spill fire area and $\dot{m}$ is the mass burning rate per unit area (kg/m^{2}s),

$$\dot{m} = A \cdot \dot{y} \cdot \rho \tag{65.13}$$

where $\dot{y}$ is the fuel burning regression rate (m/s) and ρ is the density of the fuel. The regression rate is the rate at which the fuel surface descends in a vertical direction as it burns; values are often reported in units of mm/min and therefore must be converted to m/s for the above calculations. Both, $\dot{m}''$ and $\dot{y}$ are empirically based values that are related per Equation 65.14:

$$\dot{m}'' = \dot{y} \cdot \rho \tag{65.14}$$

The literature has presented data for both parameters and both are presented below. The most commonly referenced database was developed by Blinov and Khudiakov [42] for pool fires and presented by Hottel [43] as shown in Fig. 65.19, which shows the regression rate and flame height results for various fuels burning in a broad range of pan sizes, 0.004–23 m in diameter. The data indicate that the fuel regression rate is approximately constant at 4 mm/min for all fuels tested burning as confined pool fires with diameters greater than 1 m. For smaller diameter fires, there is considerable difference in regression rates for the fuels presented. Hottel [43] discusses the trends in the burning rate data based on the balance of heat transfer to the fuel.

For fire sizes greater than about 1 m in diameter, the dominant mode of heat transfer to the liquid is via radiation from the plume. For smaller sizes, heat conduction from the pan (walls) or the substrate and convective heat transfer will constitute a larger fraction of the heat transferred to the liquid, thus having a larger effect on the burning rate of the fuel. Hottel [43], Burgess, Strasser, and Grumer [44], and Burgess, Grumer, and Wolfhard [45] present detailed discussions on these heat-transfer effects. At larger diameters (typically 1–2 m), the burning fuel regression rate tends to level out at a constant maximum value, $\dot{y}_{\max}$. For these pools in the radiation dominant region, Burgess et al. [44] with the U.S. Bureau of Mines correlated the maximum regression rates of various single-component burning fuels (pan fires) based on the thermochemistry of the liquids as follows:

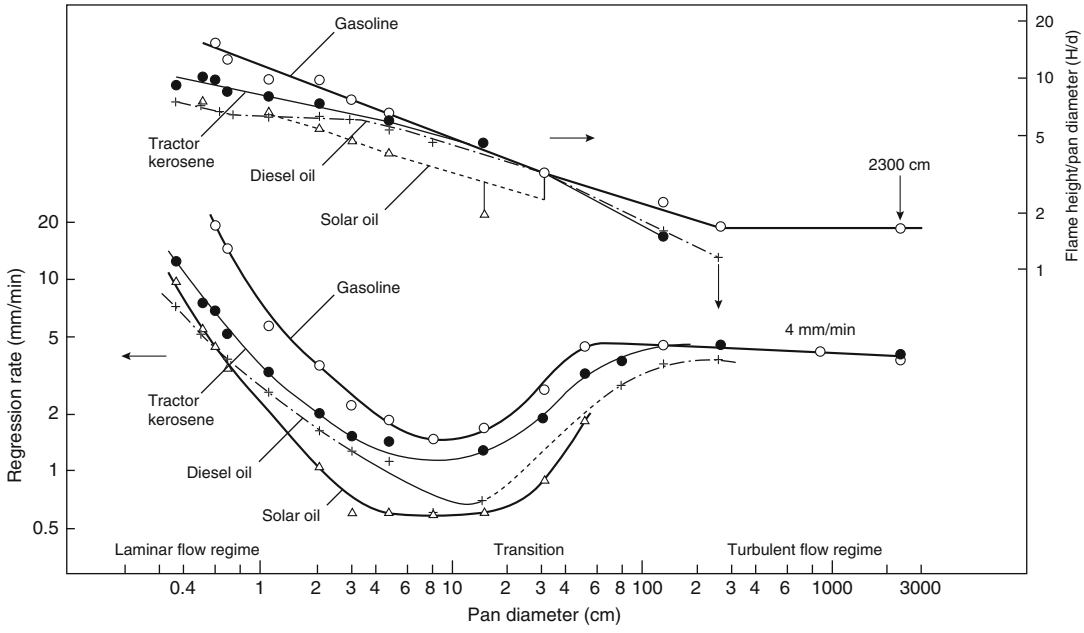

Fig. 65.19 Regression rate and flame height data for liquid pools (From Blinov and Khudiakov [42])

$$\dot{y}_{\max} = 1.27 \times 10^{-6} \frac{\Delta h_c}{\Delta h_{v,\text{sen}}} (\text{m/s}) \qquad (65.15)$$

where Δh_c is the heat of combustion and $\Delta h_{v,\text{sen}}$ is the sensible heat of vaporization, calculated as

$$\Delta h_{v,\text{sen}} = \Delta h_v + \int_{T_0}^{T_b} C_p dt \qquad (65.16)$$

where

Δh_v = Heat of vaporization at the boiling point, T_b

C_p = Specific heat of the liquid fuel

T_o = Initial temperature of the liquid

The use of the sensible heat of vaporization accounts for the temperature dependence of the regression rate, which will vary appreciably (up to tens of percent) from the value calculated using only Δh_v. As the correlation expressed by Equation 65.15 suggests, the fuel regression rate is not constant for all fuels at larger diameters as indicated for the limited fuels in Fig. 65.19. Based on a broad range of hydrocarbon pan fires, Zabetakis and Burgess [46] fit Equation 65.15 to the data shown in Fig. 65.20. The fit is quite good except for the cryogenic fuels, liquefied natural gas and liquefied propane gas. It is noted that the data apply to single-component fuel fires burning in unvitiated air under calm conditions (e.g., no wind).

Further work by the Bureau of Mines researchers, Grumer et al., [48], suggested that the regression rate for blended fuels can be represented by the same correlation (Equation 65.15) when the heats of combustion and vaporization are presented as shown in Equation 65.17 for each component of the fuel.

$$\dot{y}_{\max} = 1.27 \times 10^{-6} \left[\frac{\sum_{i=1}^{N} n_i \Delta h_q}{\sum_{i=1}^{N} n_i \Delta h_{vi} + \sum_{i=1}^{N} m_i \int_{T_0}^{T_b} C_p(T) dt} \right] \qquad (65.17)$$

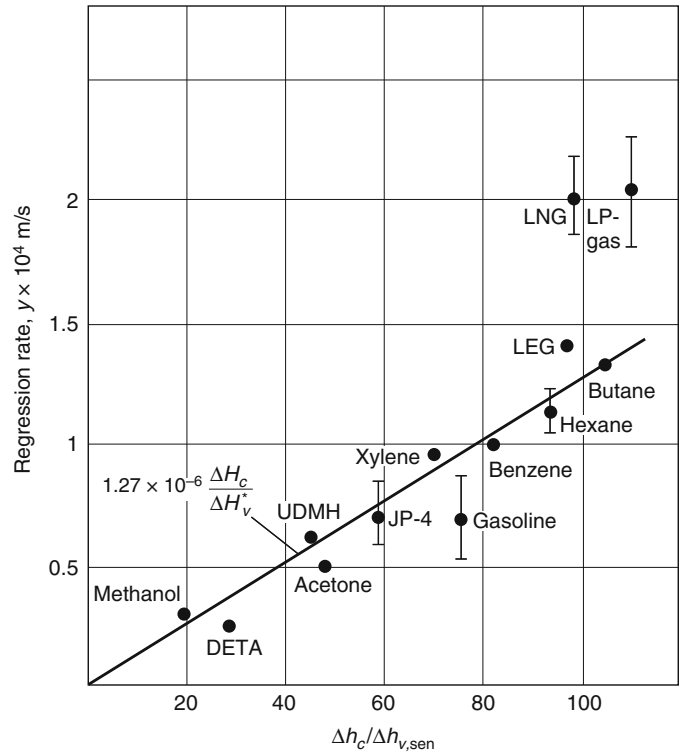

Fig. 65.20 Burning fuel regression rate plotted versus thermochemical properties of fuels burning as pan fires (Taken from Mudan [47])

where n_i and m_i are the mole fraction composition in the vapor and liquid phases, respectively.

A blended fuel with components of widely varying volatility will not burn at a uniform rate. Initially, the high volatile components will burn, and as time proceeds the burning will become more characteristic of the remaining lower volatile components. For blends such as gasoline that have components with similar heats of combustion and heats of vaporization and $n_i \approx m_i$ Equation 65.17 can be represented by

$$\dot{y}_{\max} = n_1 \dot{y}_1 + n_2 \dot{y}_2 + \ldots \qquad (65.18)$$

Equation 65.18 has been reported to yield good estimates of the regression rate for multicomponent fuel blends [48]. Even for blends with widely varying boiling points, Equation 65.18 provides rough estimates except for the initial and final stages of the fire.

Converting the regression rate data of Fig. 65.20 via Equation 65.14 allows the corresponding maximum mass burning rate per unit area, $\dot{m}''_{\max}$, to be plotted against the ratio of the heat of combustion to the heat of vaporization (Fig. 65.21). The fit to the data is represented by

$$\dot{m}''_{\max} = 1 \times 10^{-3} \frac{\Delta h_c}{\Delta h_{v,\,\text{sec}}} = \text{kg/m}^2\text{s} \qquad (65.19)$$

The fit of Equation 65.19 to the burning rate data is not as good as Equation 65.15 to the regression rate data. However, Equation 65.19 does cover a wider range of fuels, including the liquefied gases.

The regression rate is particularly useful for confined pool fires of significant depth. For many spills, particularly continuously flowing fuels, the more useful quantity is the mass burning rate per unit area. As noted in the previous discussion, the burning rate of pool fires with diameters greater than 0.2 m (see Fig. 65.19) increases with increasing diameter. Zabetakis and Burgess [46] developed the following relationship to represent the burning rate per unit area as a function of pool diameter, D:

$$\dot{m}'' = \dot{m}''_{\max}[1 - \exp(-k\beta D)] \qquad (65.20)$$

where the product $k\beta$ is represented as a single value. k is the extinction coefficient (m^{-1}) and ® is the mean-beam-length correction. The maximum steady-state burning rate per unit area, $\dot{m}''_{max}$, is also referred to in the literature by Babrauskas [49] as $\dot{m}''_{\infty}$, the mass burning rate for an infinite-diameter pool. If a confined pool is not circular, D is equal to the effective diameter, expressed as

$$D = \left(\frac{4A}{\pi}\right)^{1/2} \tag{65.21}$$

where A is the area of the pool.

Other than the data presented in Fig. 65.21, the most comprehensive collection of burning rate data has been compiled by Babrauskas [49] and is presented in Table 26.13 in Chap. 26, "Heat Release Rates." The correlation presented by Equation 65.20 agrees extremely well with the experimental data of some fuels, such as gasoline. The greatest disagreement occurs for alcohol fuels for which Babrauskas proposes a set of constant values for different diameter ranges (see Chap. 26) [50]. Due to difficulties in experimentally evaluating the cryogenic fuels, there tends to be more scatter in the data, and thus not as good a correlation with Equation 65.20 as seen for other hydrocarbon fuels.

The use of Equation 65.20 applies to confined pool fires burning in the open, under still-air conditions and in a vessel (e.g., pan or tank) without an excessive lip height [49]. The burning rate correlations presented have been developed from confined pool fire experiments. There generally has been limited data available for burning rates of unconfined fuel spill fires.

Gottuk et al. [4] conducted a series of JP-8 and JP-5 fuel spill fires on a smooth polyurethane-coated concrete slab, as used in Navy aircraft hangars. The spill fires consisted of both continuously flowing fuel releases (~0.4, 0.8, and 1.7 L/min) and 1–3 L of fixed quantities of fuel that were poured onto the concrete, allowed to spread

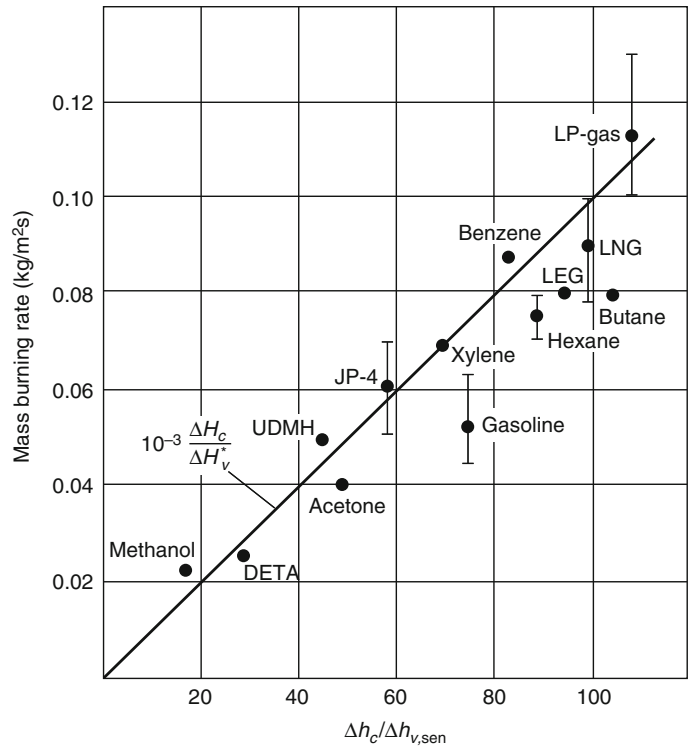

Fig. 65.21 Mass burning rate per unit area versus the thermochemical property of fuels burning as pan fires (Taken from Mudan [47])

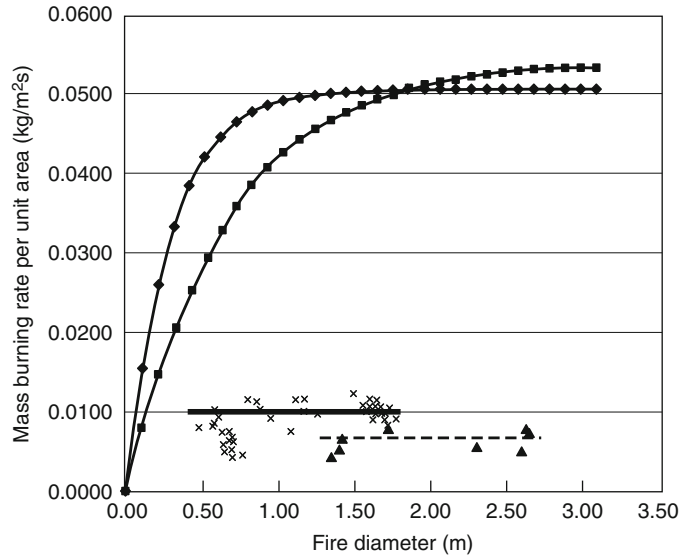

Fig. 65.22 Mass burning rates for unconfined JP-8 spill fires on concrete: [4] (x) denote 0.4–1.7 L/min continuous spill fires with an average value (—) for diameters >1.5 m; (▲) denote 1–3 L fixed-quantity spills with an average value (– – –) for diameters >1.5 m; the calculated pool fire burning rates per Equation 65.20 are shown for JP-4 (—◆—) and JP-5 (—■—)

to nearly a maximum size, and then ignited at the edge of the spill. The burning rate per unit area data for the unconfined spill fires are presented in Figs. 65.22 and 65.23 for both JP-8 and JP-5, respectively. Figures 65.22 and 65.23 show the experimentally measured $\dot{m}''$ for each test versus the measured diameter of the spill fires. Also included for comparison are the curves for burning rate for pool fires as calculated per Equation 65.20, using the data of Table 26.13. A curve for JP-8 does not appear in Fig. 65.22, due to a lack of experimental pool fire data. However, it is expected, based on fuel property data, that the burning rate curve for JP-8 is bounded by the curves for JP-4 and JP-5.

Putorti et al. [5] investigated gasoline spill fires on parquet and vinyl flooring substrates and various carpets. These fires consisted of fixed quantity (0.25–1.0 L) spills that were ignited approximately 60 s after release. Consistent with the results for the JP-8 and JP-5 spill fire data noted above [4], the burning rates for gasoline on the nonabsorbing materials were found to be one-fifth that of the maximum rate for pool fires (i.e., ~80 % reduction). Based on these limited fuel spill fire data, the previous edition of this chapter suggested that burning rates for unconfined liquid fuel spills be estimated as one-fifth of the maximum pool burning rate. At the time, the actual mechanism for this large difference was not known, but had been hypothesized to be primarily due to differences in heat transfer between the fuel and substrate for spills compared to deeper pools. Since the last edition of this chapter, work has shown this hypothesis to be incorrect [8].

A more recent test program conducted by Mealy, Benfer and Gottuk [8] has provided additional insight regarding the burning dynamics of unconfined fuel spills compared to pool fires. A series of tests evaluated the burning dynamics of multiple fuels (gasoline, kerosene, denatured alcohol), at various depths (0.5–20 mm), on multiple substrates (concrete, wood, vinyl, steel, water). Several different fuel supply scenarios were also considered: fixed quantity pool fires, continuously flowing spill fires, and fixed quantity spill fires. Based upon the testing conducted, the burning rate of a liquid fuel spill/pool fire was determined to be primarily dependent upon several factors, including, fuel depth, fuel supply duration and substrate.

Fuel depth was identified as a factor because it is directly related to the fuel supply duration for fixed quantity/fixed area fires (i.e., a pool fire). For these scenarios, a depth of 5 mm represents the minimum depth for which a peak, steady-state mass burning rate comparable to the

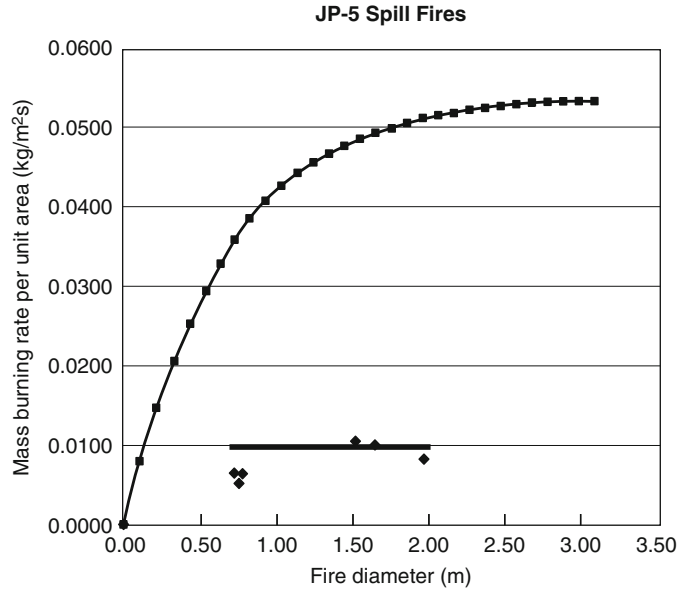

Fig. 65.23 Mass burning rates for 0.4–1.7 L/min unconfined JP-5 spill fires on concrete (◆) [4]. The average value for diameters >1.5 m is shown as (—); the calculated pool fire burning rate per Equation 65.20 is shown as (—■—)

diameter dependent maximum mass burning rate (see Equation 65.20) has sufficient time to be achieved. This was true for steel, water, concrete, and vinyl substrates. At depths less than 5 mm, the peak burning rates were consistently less than the diameter dependent maximum burning rate. This reduction in peak burning rate (also presented as heat release rate per unit area, HRRPUA, of fuel surface) can be seen in Fig. 65.24, which shows burning rates for six pan fires of gasoline with increasing fuel depths from 1 to 18 mm. As can be seen, until the depth reached 5 mm, the fire did not burn long enough to achieve the steady-state peak burning rate as achieved at the 18 mm depth, which burned for over 6 min. At the shallower depths approaching unconfined spill fires (~1 mm), the fires burned for less than a minute, which is typical for a spill fire.

The reduction in mass burning rate associated with a 1 mm fuel depth was on the order of 70–80 %, equivalent to the trends observed by the previous studies [4, 5] noted above. The results of spill fire tests are summarized in Table 65.4. Based upon the data collected, correlations were developed for both gasoline and kerosene that can be used to predict the reduction in peak mass burning rate as a function of fuel depth and fuel area:

$$C_\delta = 0.95^*\left(1 - e^{-0.71\delta}\right) \quad \text{for gasoline} \tag{65.22a}$$

$$C_\delta = 0.91^*\left(1 - e^{-0.58\delta}\right) \quad \text{for kerosene} \tag{65.22b}$$

where C_δ is the depth coefficient and δ is the calculated fuel depth (mm). However, to date, depth coefficient correlations have only been developed for gasoline and kerosene fuels. If depth coefficients for other fuels are required it is recommended that either Eq. 22a or 22b be used based on similar properties or an average coefficient of 0.69 be used for spill depths $\leq$5 mm and a coefficient of 1.0 be used for spill depths >5 mm.

The product of these depth correlations with the diameter dependent mass burning rate correlation (Equation 65.22) provides a more accurate prediction of mass burning rates for thin fuel layer fire scenarios:

$$\dot{m}''(D,\delta) = C_\delta^*\left(\dot{m}''_\infty\left(1 - e^{-k\beta D}\right)\right) \tag{65.23}$$

Although the 5 mm depth criterion is appropriate for all fixed quantity scenarios, the same is not true for continuously-fed fire scenarios. For continuous-fed spills, Mealy et al. maintained

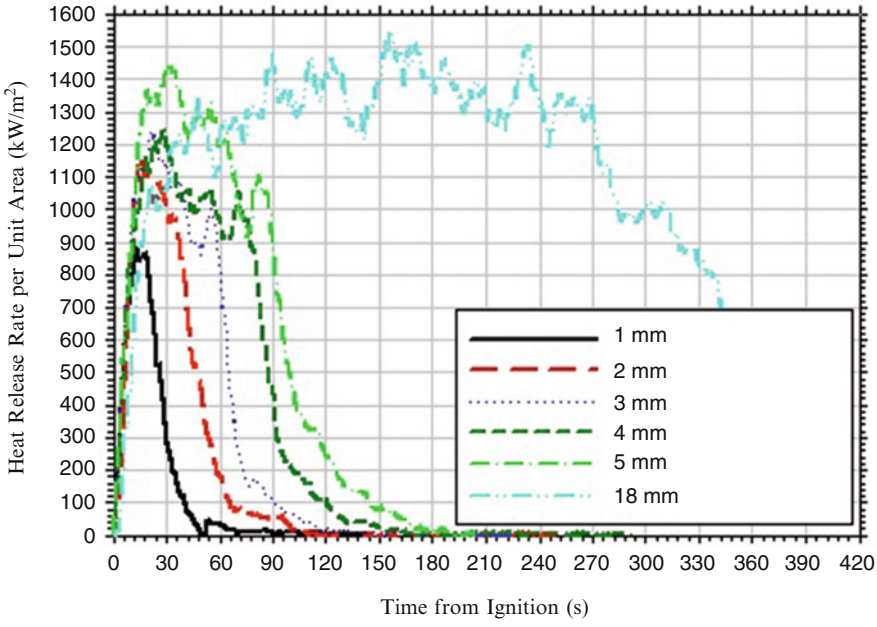

Fig. 65.24 Summary of HRRPUA data measured for gasoline on water in 1.5 m^2 (16 ft^2) pan fire tests with fuel depths of 1, 2, 3, 4, 5 and 18 mm

Table 65.4 Peak burning rates for unconfined fuel spill fires

Description	Peak mass burning rate per area (kg/m^2s)	Standard deviation	Reference
JP-8			
1–3 L spills	0.007[a]	0.0014	Gottuk et al. [4]
0.4–1.7 L/min spills	0.010[a]	0.0009	Gottuk et al. [4]
JP-5			
0.4–1.7 L/min spills	0.010[a]	0.0008	Gottuk et al. [4]
Gasoline	0.011	–	Putorti et al. [5]
Gasoline	0.016[b]	–	Mealy et al. [8]
Kerosene	0.010[c]	–	Mealy et al. [8]
Denatured alcohol	0.014[d]		Mealy et al. [8]

[a]Represents average for fires with diameters greater than 1.5 m burning for a maximum of 3 min
[b]Represents average for fires with diameters between 0.75 and 1.45 m
[c]Represents average for fires with diameters less than 0.75 m
[d]Represents average for fires with diameters less than 0.6–3.0 m

fuel depths on the order of 1 mm while still achieving peak mass burning rates that were comparable to the diameter dependent maximum mass burning rates. These results further demonstrate that it is not the depth of fuel that impacts the peak mass burning rate, but that it is the duration of fuel supply. If the fuel supply is sufficient to allow enough time to reach a steady-state, than the maximum mass burning rate is achievable. In addition to the impact of fuel supply duration on the burning rate of combustible fuels, specifically kerosene and diesel, the ignitability and flame spread potential of the fuel at thin depths is very small, making the fuel very challenging to ignite and burn in a thin depth spill scenario without a large external heat exposure.

An additional parameter identified as having an impact on the mass burning rate of a fuel was

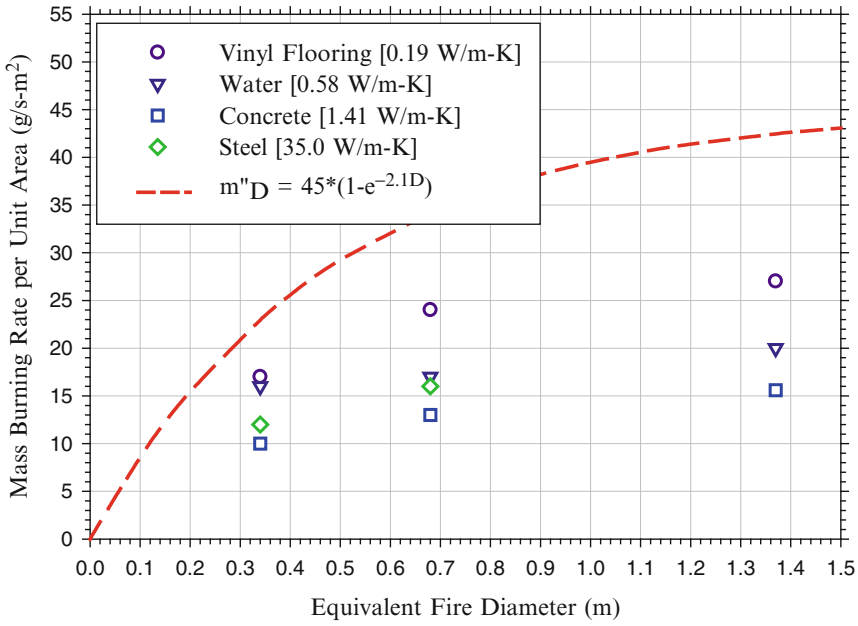

Fig. 65.25 Comparison of peak mass burning rates per unit area for 1 mm (0.04 in.) gasoline fires on substrates with various thermal conductivities (shown in *brackets*) [8]

the substrate on which the fuel is burning. However, the influence of the substrate was only found to be significant for fuel depths less than 5 mm. The data collected by Mealy et al. [8] showed differences in the mass burning rates of 1 mm depth liquid fuels burning on surfaces with differing thermal properties (Fig. 65.25). The rank order of the mass burning rates for each fire size were consistent with the highest burning rates occurring on vinyl flooring and the lowest on concrete. For the scenarios evaluated, no specific thermal property of the substrates (i.e., thermal conductivity, thermal inertia, thermal effusivity, and thermal diffusivity) could be directly correlated to the rank order of burning rates. In general, less thermally conductive materials (i.e., vinyl and water) produced mass burning rates higher than those achieved in tests with more thermally conductive substrates (i.e., steel and concrete). However, the ranking of mass burning rates with respect to the thermal conductivity of the substrates was not appropriate when evaluating the case of the concrete and steel. In this case, the mass burning rates measured on the concrete were consistently lower than those measured on the steel despite the fact that the thermal conductivity of steel is an order of magnitude larger than that of concrete. This discrepancy may be attributed to the reflectivity of the steel and the resulting re-radiation from the steel substrate to the fuel layer. This reflected heat would then be transferred into the fuel layer thus raising the mass burning rate of the fuel.

Empirical data has also shown that a delay in ignition time of a fixed quantity fuel spill can have a significant effect on the peak fire size obtained. Changing the ignition delay (i.e., the time between the spill and the ignition of the fuel) from 30 to 300 s produced an average reduction in fire size (burning rate) of approximately 50 % for 0.5 and 1 L gasoline and denatured alcohol spill fires [8]. The primary impact of longer ignition delay times is the result of shallower fuel depths due to a combination of larger spill areas and prolonged periods of evaporation. Given that most fuel spill fires nominally burn out in less than 1–2 min, longer ignition

delay times can lead to both lower peak heat release rates and shorter duration fire exposures that are quite fast events.

Based on Equations 65.11 and 65.12, the heat release rate of an unconfined spill or confined pool fire can be calculated per Equation 65.24 once the area of the fire is determined and an appropriate mass burning rate per area is identified.

$$\dot{Q} = \dot{m}'' \cdot A \cdot \Delta h_c \tag{65.24}$$

However, in the case of an unconfined, continuously flowing spill fire, the area is neither known a priori nor can it be calculated per any fuel depth correlations as with a fixed quantity spill. As fuel flows from a continuous source, the size of the resulting spill will continue to increase indefinitely until a physical boundary is reached or the fuel is ignited and burns. The transient nature of a continuous spill fire is very dependent on the timing of the fuel ignition and the flame spread rate relative to the fuel flow rate and size of the spill at the time of ignition. For example, if a continuously flowing spill is immediately ignited at the source, the fire size will be equal to the spill size if the flame spread rate is faster than the fuel spill spread rate. However, if the fuel spill spread rate is faster than the flame spread rate, the spill will continue to spread out ahead of the flame front.

As discussed below, a continuously flowing spill fire will reach a steady-state burning size, characterized by the equivalent steady-state diameter, D_{ss}. It is possible for a fuel spill to reach a diameter that is larger than D_{ss} before it is ignited. In this case, the flame will spread across the fuel surface to the larger diameter and then the spill fire will reduce in size until D_{ss} is reached. These examples are only several of multiple scenarios that can occur. Currently, complete and accurate models of burning fuel spills do not exist. In order to estimate the transient nature of a continuous fuel spill fire, the engineer must consider the fuel spill rate, the relative time of ignition, and the steady-state burning spill area.

The steady-state burning spill area, A_{ss}, results due to a balance between the volumetric flow rate of the liquid release, $\dot{V}_L$ (m^3/s), and the volumetric burning rate of the fire as described by

$$\dot{V}_L = A_{ss} \cdot \dot{y} = \frac{\pi {D_{ss}}^2}{4} \dot{y} \tag{65.25a}$$

or, alternatively in terms of the mass burning rate as

$$\dot{V}_L = A_{ss} \frac{\dot{m}''}{\rho} = \frac{\pi {D_{ss}}^2 \dot{m}''}{4\rho} \tag{65.25b}$$

The steady-state size of the spill can be explicitly solved by rearranging Equations 65.25a and 65.25b in terms of D_{ss} (m):

$$D_{ss} = \left(\frac{4\dot{V}_L}{\pi \dot{y}}\right)^{1/2} \tag{65.26a}$$

$$D_{ss} = \left(\frac{4\dot{V}_L \rho}{\pi \cdot \dot{m}''}\right)^{1/2} \tag{65.26b}$$

The calculation of the spill size per Equation 65.26 assumes that all fuel is burned from the spill; that is, there are no other losses of fuel from the spill, such as into a porous substrate. As noted by the examples above, D_{ss} does not necessarily correspond to the maximum fire size but equals the size of the fire once the burning rate becomes constant and equilibrium conditions are reached.

Empirical correlations can also be used to calculate the equivalent diameter of a continuous spill fire. Mansfield and Linley [51] developed a correlation for the burning spill diameter as a function of fuel flow rate for large release rate fires on concrete. The following correlation was developed for 568–2271 L/min (150–600 gpm) continuous spill fires of JP-5 ranging in size from 15 to 24 m in diameter:

$$D_{ss} = 134\left(\dot{V}_L\right)^{1/2} : D_{ss}\,(\mathrm{m}) \text{ and } \dot{V}_L\left(\mathrm{m}^{3/5}\right) \tag{65.27a}$$

$$D_{ss} = 3.5\left(\dot{V}_L\right)^{1/2} : D_{ss}\,(\mathrm{ft}) \text{ and } \dot{V}_L(\mathrm{g\,pm}) \tag{65.27b}$$

where 1 m^3/s = 15,850 gpm.

The tests of Mansfield and Linley [51] were conducted outside with 2.2–12.5 m/s (5–28 mph)

winds and ambient temperatures ranging from 7 °C to 32 °C. Using Equation 65.25b with the diameter and spill rate data of Mansfield and Linley [51], the mass burning rate per unit area of the large JP-5 continuous spill fires is calculated to be in the range of 0.055 kg/m^{2}s, which agrees with the pool fire burning rate data reported by Babrauskas [50] in Table 26.21 of this handbook. As noted above, despite typical spill depths of about 1 mm and less, continuous flowing spill fires will reach the peak (steady-state) mass burning rate if allowed to burn long enough.

In order to assess the thermal threat associated with a fuel spill/pool fire scenario, the peak fire size must be coupled with exposure duration. Estimating exposure duration can be accomplished using one of two techniques. The first technique assumes that the peak fire size is reached instantly and is maintained so long as fuel is present. Using this technique, the burning duration for a given fire scenario can be calculated using Equation 65.28.

$$t_b = \frac{4m}{\pi D^2 \dot{m}''_\infty} \qquad (65.28)$$

where t_b is the burning duration for a given scenario (s), m is the mass of fuel available to burn (kg [lbs.]), D is the effective spill diameter (m [ft]), and $\dot{m}''_\infty$ is the peak mass burning rate per unit area for the given fuel (g/s-m^2 [lbs./s-ft^2]). Traditionally, many have assumed that the peak heat release rate of a liquid fuel fire is reached instantaneously and maintained for the duration of the fire as calculated via Equation 65.28. Consequently, the exposure times associated with this assumption are most likely underestimated as shown in Fig. 65.26 as the "predicted" curve. In general, this approach tends to over-predict the peak thermal exposure resulting from a fuel spill/pool scenario.

The second technique that can be used to approximate the transient behavior of a fire resulting from the ignition of a liquid fuel spill/pool is to characterize the development, peak, and decay of the fire. This is accomplished by approximating the spread velocity on the hydrocarbon pool surface from the point of ignition, the time to develop maximum burning conditions, and the time to consume all fuel at a

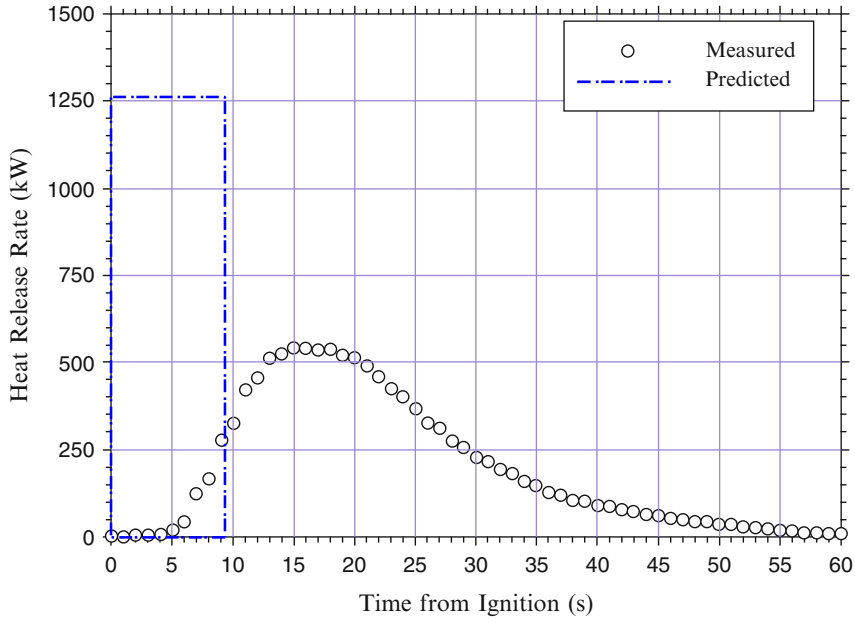

Fig. 65.26 Comparison of measured and predicted spill fire heat release rates using assumption that peak heat release rate is achieved instantly [8]

given location. Mealy et al. provide a methodology for estimating the fire growth and decay [8].

For liquid pool fires (depths ≥0.5 mm), although the entire fuel surface may be fully involved, the burning rate per area (or regression rate) will increase over time until the maximum steady-state value is reached [46]. The transient time period may be tens of seconds to minutes, depending on the type of fuel, the fuel depth, and the bounding materials (e.g., building walls or metal tank). During this transient period, the temperature gradient in the fuel is being established. Once the fuel surface reaches the boiling temperature, the burning rate approaches the steady-state value. If a transient analysis of a fire is required, further consideration must be given to the mass burning rate (or regression rate) that is selected. The use of the maximum value may not be appropriate for the entire burning duration.

Other Factors and Limitations

The spill areas and burning rates of liquid spill or pool fires presented in this chapter have been developed from experimental data of fires on level surfaces. In many applications, fuel spills will occur on inclined and/or cluttered surfaces. Under these conditions, fuel spread will ultimately be dependent on the geometry of the surface, which may lead to pooling of the fuel, channeling, and/or larger wetted areas than would occur on a level surface. Fuel flowing on an inclined surface can result in faster and wider spread of fire. No published studies have evaluated the impact of three-dimensional fuel flow on spill fire burning rates.

This chapter has primarily addressed the burning of liquid fuel fires that occur in the open. Liquid fuel fires in enclosures were studied by Mealy et al. [52] and showed that spill fire scenarios are unaffected by the enclosure (assuming sufficient air supply) since the duration of a spill fire is quite short. However, pool fires in an enclosure have been shown to have enhanced burning (~60 %) relative to open burning when a radiating upper layer is created in the compartment fire [52]. This increase can be moderated by restricted ventilation to the compartment, which can decrease the mass burning rate of a pool fire.

Babrauskas [49] and Zabetakis and Burgess [46] have reported that burning rates of pool and spill fires both increase and decrease under increased wind speeds. Burgess and Hertzberg [53] reported that wind speeds increased the burning rate for small-diameter fires; however, burning rates never exceeded the maximum burning rate in still air corresponding to larger diameter fires. High wind speeds can cause fuel to spill out of contained areas or cause unconfined spill fires to move in the direction of the wind. At higher wind speeds, flames can also be blown off.

For pool fires in pans or tanks, the lip height can impact the burning rate of the fuel. There is limited data on this topic and experimental results show both an increase and decrease in the burning rate with larger lip heights [49]. Much of the experimental data have been for small pan diameters (<1 m) (e.g., Emmons [54]).

Flame Height

The flame height of a liquid spill or pool fire can be calculated based on a number of experimental correlations [55]. The following correlation developed by Heskestad [55] has been shown to be quite robust for different fuels over a wide range of pool fire sizes:

$$L_f = 0.23\dot{Q}^{2/5} - 1.02D \qquad (65.29)$$

where

L_f = The 50 percentile intermittent flame height (m)

$\dot{Q}Z$ = The heat release rate (kW)

D = The diameter of the fire (m)

The use of Equation 65.29 to characterize unconfined spill fire heights was evaluated by Gottuk [4] for JP-8 and JP-5 spill fires on concrete. The results of the comparison are shown in Figs. 65.27 and 65.28, which present measured intermittent flame heights (50 percentile) and

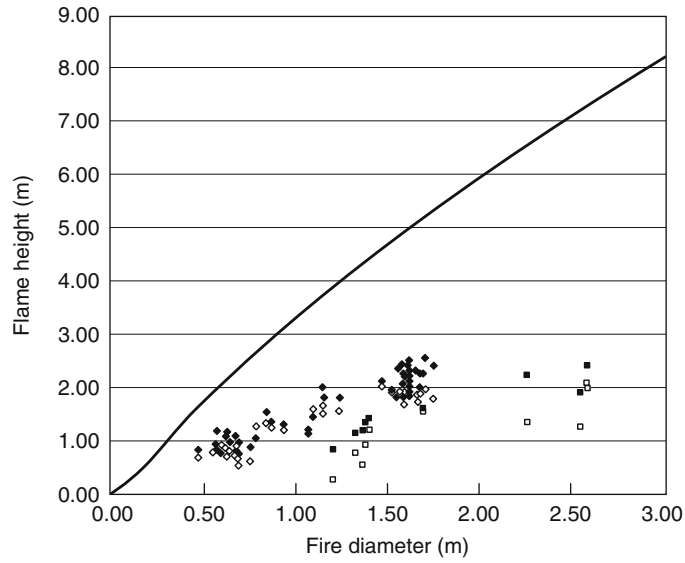

Fig. 65.27 Comparison of measured and predicted flame heights for unconfined JP-8 spill fires: [4] measured (◆) and predicted (◇) 0.4–1.7 L/min continuously flowing spill fires; measured (■) and predicted (□) 1–3 L fixed-quantity spill fires; and predicted pool fires (——)

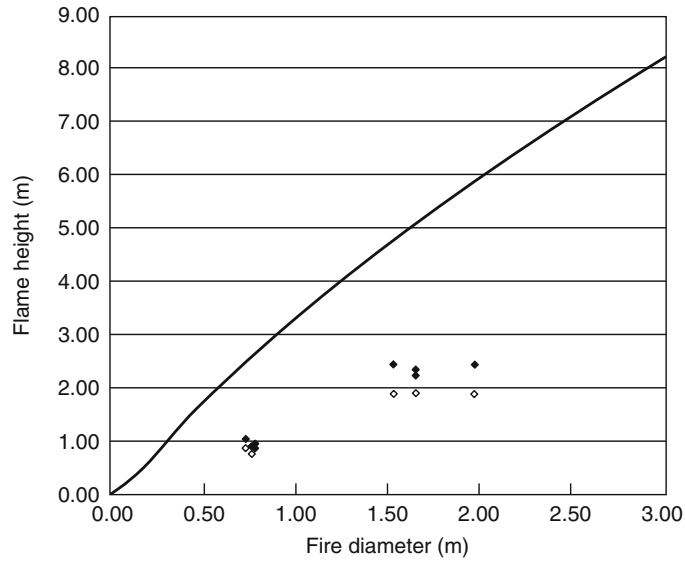

Fig. 65.28 Comparison of measured and predicted flame heights for unconfined JP-5 spill fires: [4] measured (◆) and predicted (◇) 0.4–1.7 L/min continuously flowing spill fires; and predicted pool fires (——)

predicted flame height values plotted versus the spill diameter. For comparison, the predicted flame heights of pool fires are also plotted as a curve in each figure. The predicted pool fire heights are based on Equation 65.29 and pool burning rate data of Table 26.13. Consistent with the difference in the mass burning rates between spill and pool fires, the spill flame heights are considerably shorter than those for pool fires of the same diameter. Using the Heskestad flame height correlation (Equation 65.29) with the spill fire data yields predicted heights that are approximately 17 % lower compared to the measured spill fire flame heights. For most engineering applications, the Heskestad flame height correlation (Equation 65.29) provides satisfactory predictions for both liquid pool and spill fires.

Fire Hazard Analysis Framework

When conducting fire hazard analyses, fuel type and spill/pool configuration parameters are often user selected and/or varied to assess a wide range of fire scenarios. In this case, the user would identify the fuels of interest and obtain the relevant fire property data. Four different scenarios are identified for fire hazard analyses based upon the identification of confined and unconfined spill scenarios and fixed quantity and continuously-fed fuel supplies. These four paths generally encompass the vast majority of potential liquid fuel scenarios and require different analytical approaches to understand the resulting fire threat. The approach presented will lead to the calculation of the largest possible fire size. It is important to note that in some analyses, a smaller fire size that lasts longer may actually be a worst-case of more challenging fire hazard. The discussion above can be used to assess such scenarios (Fig. 65.29).

The first spill/pool scenario considered was a fixed quantity of fuel in a confined area. For the purposes of this discussion, it is assumed that the quantity of fuel is such that it covers the entire area of confinement otherwise it is considered as a fixed quantity, unconfined scenario. Based upon this assumption, an equilibrium spill depth can be calculated using the known volume of

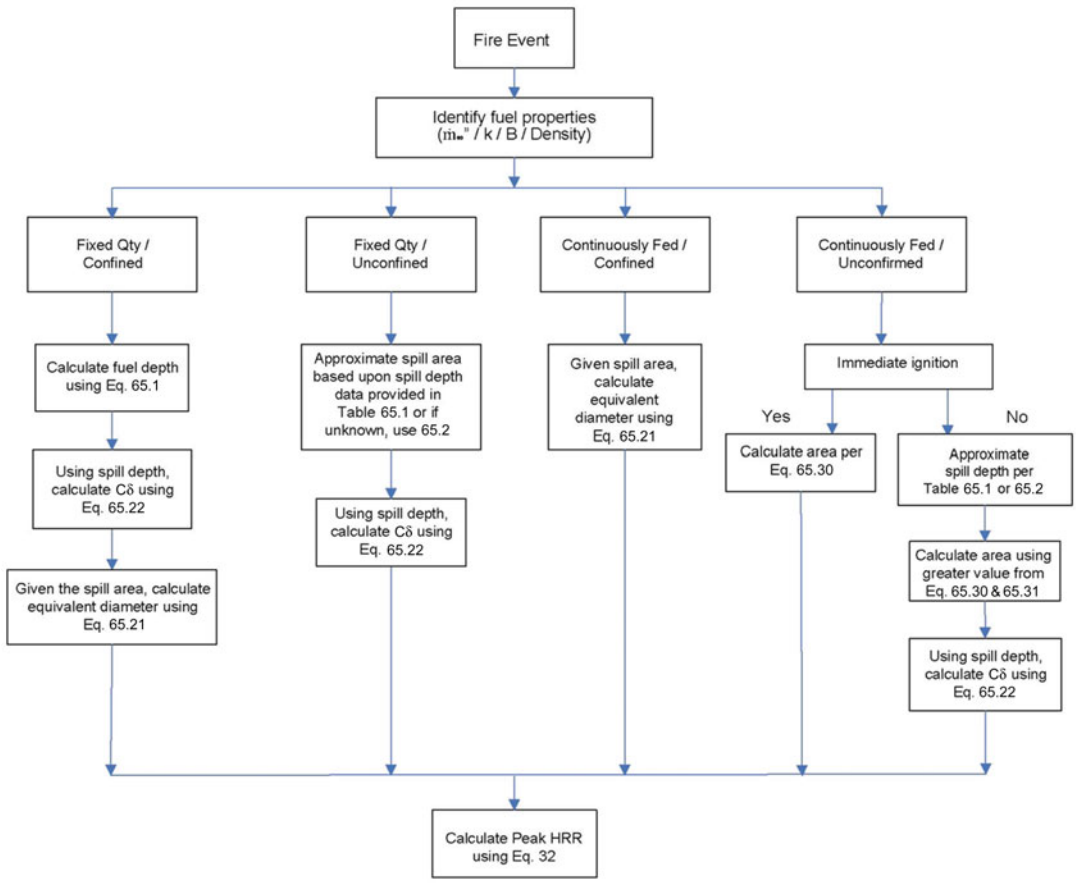

Fig. 65.29 Analytical framework for characterizing fuel spill/pool fire scenarios from a fire hazard viewpoint

liquid spilled and the area of confinement as shown in Equation 65.1.

$$\delta = \frac{V_o}{A_o} \tag{65.1}$$

where δ is the fuel depth (mm [ft]), Vo is the volume of liquid (L [gal.]), and the A_o is the area of confinement (m^2 [ft^2]).

The second scenario considered is a fixed quantity spill that is unconfined. In this scenario, the bulk flow of the liquid as well as the length of time between the spill and the ignition of the liquid dictates the area covered as opposed to bounding obstacles inhibiting the flow. For a specific spill scenario in which the substrate and/or ignition delay times are known, more representative spill depths can be approximated using the data provided in Table 65.1 (and Table 7.1 of Ref. [4]). Otherwise Equation 65.2 recommended for guidance:

$$\delta = 0.7 \text{ mm for most fuels and conditions} \tag{65.2a}$$

$$\delta = 2.9 \text{ mm for quantities of 38 L (10 gal) where analysis warrants longer duration fires} \tag{65.2b}$$

Once an appropriate spill depth has been determined, the area of coverage for a given quantity spill can be calculated using Equation 65.1. Similarly, if the area of coverage is known and a fuel depth is assumed, one can approximate the quantity of liquid spilled using Equation 65.1.

The next scenario considered is a continuously-fed, fixed area (i.e., confined) fuel supply. In this scenario, it is assumed that the fuel supply rate is equal to or greater than the mass burning rate, such that a fixed area of some depth is maintained for an extended period of time. It is also assumed that the fuel does not overflow the confined area. In this scenario, the area is known and the depth of fuel is not important given that fuel is continuously supplied, and thus burn-out does not occur (i.e., steady-state burning is allowed to develop).

The final scenario identified is a continuously-fed, unconfined spill scenario. For this scenario, it necessary to identify the time of ignition given that this time will dictate the initial spill area. To address this parameter, two paths are possible. The first path assumes ignition immediately upon release of the liquid. Once ignited, the burning area of fuel will grow in size until an equilibrium spill area is achieved, which will occur when the fuel burning rate equals the fuel supply rate. Equation 65.32 represents the balance between these rates (based on Equation 65.25).

$$A_{ss} = \frac{\rho \dot{V}_L}{\dot{m}''} \tag{65.30}$$

where A_{ss} is the equilibrium spill fire burning area (m^2 [ft^2]), $\dot{V}_L$ is the volumetric fuel supply rate (m^3/s [ft^3/s]), ρ is the fuel density (kg/m^3 [lbs./ft^3]), and $\dot{m}''$ is the mass burning rate per unit area (kg/s-m^2 [lbs./s-ft^2]). Once this equilibrium solution is obtained, the maximum area of the spill is known, and the depth of fuel is not important given that fuel is continuously supplied and burning will reach a steady-state.

The other path identified for the continuously-fed, unconfined scenario is a delayed ignition (i.e., liquid is permitted to spill and spread for some period of time prior to ignition). As shown in Equation 65.31, in this scenario, the area of coverage of the spilled liquid prior to ignition can be determined based upon the product of the volumetric flow rate, $\dot{V}_L$, the ignition delay time, and an assumed spill depth.

$$A_t = \frac{\dot{V}_L t}{\delta} \tag{65.31}$$

where A_t is the spill area (m^2 [ft^2]) at a given point in time, $\dot{V}_L$ is the volumetric fuel supply rate (kg/s [lbs/s]), t, is the time in seconds after the spill occurs prior to ignition, and δ is the calculated fuel depth (m [ft]). Using a spill depth from Table 65.1 or the average spill depth of 0.72 mm, an initial spill area can be approximated by Equation 65.33. Once ignited,

the initial spill area will grow or regress to the equilibrium spill area, as calculated for the immediate ignition scenario with Equation 65.32. Consequently, the initial area calculated may provide the maximum fire size, but it will only last for a brief period of time as the fire regresses to the equilibrium area.

Once the spill areas and corresponding spill depths have been calculated, it is necessary in some spill scenarios to calculate the depth coefficient, a parameter developed to modify the maximum fuel burning rate based on small depths causing early burn out before steady-state burning can be achieved. The correlations developed for gasoline and kerosene are provided in Equations 65.22a and 65.22b.

$$C_\delta = 0.95^*\left(1 - e^{-0.71\delta}\right) \quad \text{for gasoline} \tag{65.22a}$$

$$C_\delta = 0.91^*\left(1 - e^{-0.58\delta}\right) \quad \text{for kerosene} \tag{65.22b}$$

where C_δ is the depth coefficient and δ is the calculated fuel depth (mm). If depth coefficients for other fuels are required it is recommended that either Eq. 22a or 22b be used based on similar properties or an average coefficient of 0.69 be used for spill depths ≤5 mm and a coefficient of 1.0 be used for spill depths >5 mm.

Once the fuel depth, fuel coverage area, and depth coefficient are determined using the methods described above, the final step in the analysis is the prediction of the heat release rate of the fire. Calculating the peak and/or transient heat release rates requires knowledge of a fuel's maximum mass burning rate per unit area ($\dot{m}''_\infty$, also seen as $\dot{m}''_{max}$), optical properties of the fire plume (kβ), and the heat of combustion of the fuel (ΔH_c). Using this fuel data, combined with the spill parameters described above, a transient heat release rate for the given scenario can be calculated. The general form for this calculation is presented in Equation 65.26 and expanded below as Equation 65.32, which calculates the peak heat release rate for a given fuel:

$$\begin{aligned}\dot{Q}_p &= C_\delta \dot{m}''_\infty \left(1 - e^{-k\beta D}\right) A \Delta H_C \\ &= C_\delta \dot{m}''_\infty \left(1 - e^{-k\beta D}\right) \frac{\pi D^2}{4} \Delta H_C\end{aligned} \tag{65.32}$$

where $\dot{Q}_p$ is the peak fire size (kW [Btu/s]), C_δ is the depth coefficient, $\dot{m}''_\infty$ is the peak mass burning rate per unit area for the given fuel (g/s-m^2 [lbs./s-ft^2]), kβ is an empirical constant specific to the fuel, A is the spill area (m^2 [ft^2]), ΔH_c is the heat of combustion of the fuel (MJ/kg [BTU/lbs.]), and D is the effective spill diameter (m [ft]). The effective diameter of non-circular spills can be calculated using Equation 65.21.

$$D = \sqrt{\frac{4A}{\pi}} \tag{65.21}$$

Equations 65.32 and 65.21 provide a means of calculating a peak heat release that is both fuel depth and fire diameter dependent. This prediction provides the largest potential fire that a given liquid fuel fire can produce.

Example 1 A 208 L (55 gal) drum of gasoline is suddenly ruptured during a warehouse accident. The fuel is released quickly across the floor of the warehouse and is ignited when it comes in contact with a piece of faulty equipment. Determine the maximum size of the resulting fire.

Solution First, the size of the spill is calculate by estimating the spill depth. Since gasoline is spilled on an unknown floor material, a depth value of 0.71 mm is selected from Table 65.1. Using Equation 65.1 and assuming that the release occurs instantaneously (i.e., the spill is nearly at its maximum diameter at the time of ignition) and is allowed to spread freely, the spill area is calculated as

$$A = V/\delta = 208\ \text{L}/0.71\ \text{mm} = 293\ \text{m}^2$$

Per Equation 65.21, the corresponding diameter of the burning spill is 19.3 m. To account for the short duration of the spill fire due to the shallow spill depth, δ, the depth coefficient is

calculated per Equation 65.22a to modify the peak mass burning rate:

$$C_\delta = 0.95^*\left(1 - e^{-0.71\delta}\right) = 0.38$$

The heat release rate for the fire is then calculated per Equation 65.32 as

$$\dot{Q}_p = C_\delta \dot{m}''_\infty \left(1 - e^{-k\beta D}\right) A \Delta H_C = C_\delta \dot{m}''_\infty \left(1 - e^{-k\beta D}\right) \frac{\pi D^2}{4} \Delta H_C$$
$$= 0.38 \cdot 0.055 \cdot (1 - \mathrm{e}\text{^}(-2.1\ \ 19.3))\,\pi\,(19.3\mathrm{m})^2/4 \cdot 43.7 = 267\,\mathrm{MW}$$

From Table 26.21, the heat of combustion of gasoline is 43,700 kJ/kg, the density is 740 kg/m^3, and the maximum mass burning rate per unit area of gasoline, $\dot{m}''_{\max}$, is 0.055 kg/m^{2}s.

The intermittent flame height is calculated per Equation 65.29 as

$$L_f = 0.23\dot{Q}^{2/5} - 1.02D$$
$$= 0.23(26.700\,kW)^{2/5} - 1.02(12.2\,m) = 5.8\,m$$

If it is assumed that the fuel spill burns at the maximum rate for the duration of the fire, the burn time, t_b, for the fuel spill fire will be only 2 min:

$$t_b = \frac{m_f}{\dot{m}''A} = \frac{V \cdot \rho}{\dot{m}''A} = \frac{0.208\,m^3 \cdot 740\mathrm{kg}/m^3}{0.021\mathrm{kg}/m^2 s \cdot 293\,m^2}$$
$$= 25\,s$$

Where the mass burning rate, $\dot{m}''$, is calculated per Equation 65.23 as

$$\dot{m}''(D,\delta) = C_\delta * \left(\dot{m}''_\infty \left(1 - e^{-k\beta D}\right)\right)$$
$$= 0.38\left(0.055\left(1 - \left(1 - e^{-21*193}\right)\right)\right)$$
$$= 0.0209\frac{kg}{m2s}$$

As illustrated in Example *2*, the predicted burn time of 25 s is most likely too short. In reality, the fire will last longer due to the fact that the flame takes time to spread across the spill.

Example 2 Consider the situation in Example *1*. What is the time required for the entire spill to become involved in the fire? The temperature in the warehouse is 20 °C.

Solution The most critical step in determining the time for the entire spill to become involved in the fire is to identify both the temperature of the liquid fuel spill and the flashpoint of the fuel. The flashpoint of gasoline is indicated to be −45 °C as documented in the third edition of the *SFPE Handbook* in Kanury's [56] table, "Selected Ignition, Flammability, and Autoignition Properties of Some Fuels in Air." Assuming that the gasoline is at the same temperature as the warehouse, 20 °C, the spill temperature is well above the closed-cup flashpoint. The elevated temperature indicates that gas phase flame spread will occur if the spill is ignited. A reasonable and generally conservative approximation of the upper gas phase flame spread velocity is 200 cm/s.

The problem statement does not specify the location of the ignition source relative to the spill. The most conservative posture for fastest involvement would be to assume that the ignition source is in the center of a circular spill. Using Equation 65.8 for circular spills will define the time for full involvement:

$$t_{A,\max} = \frac{r_{A,\max}}{v}$$

where $r_{A,\max}$ is 6.1 m and v is 2.0 m/s. The time for full involvement becomes

$$t_{A,max} = \frac{9.65}{2.0\,m/s}$$

$$t_{A,max} = 4.8\,s$$

If the ignition source was located at the perimeter of the gasoline spill, it would take approximately

10 s to travel the full 19.3 m diameter of the pool to involve the spill completely. Irrespective of the ignition location, the time to involve the entire spill is small in the context of most hazard analyses time scales. Therefore, when gas phase flame spread is governing the involvement of a spill or pool of flammable liquid, it is often acceptable to assume instantaneous ignition of the entire fuel surface. This assumption may not be valid for extremely large spills (e.g., tanker spills) or when there are short time-scale concerns.

The difference between gas phase flame spread and liquid-controlled flame spread can be illustrated by assuming that the drum of gasoline in the foregoing example contained diesel fuel. The flashpoint of diesel fuel ranges from 52 °C to 96 °C according to the 1994 edition of NFPA 325 [57]. Since the warehouse is at 20 °C, substantially below the flashpoint of diesel fuel, flame spread would be governed by liquid-controlled mechanisms. A conservative upper bound of the liquid-controlled flame spread in this case would be 10 cm/s. Assuming that the area of the diesel spill was identical to the gasoline spill and that there was a strong enough ignition source present to ignite the spill, a time to full ignition of the spill can be estimated. Assuming that the ignition source was in the center of the spill, Equation 65.8 would be used again, where the maximum radius of the spill is 6.1 m and the flame spread velocity is 0.1 m/s. The time for full involvement becomes

$$t_{A,max} = \frac{9.65}{0.1\,m/s}$$

$$t_{A,max} = 67\,s$$

The conservative estimation of the time for full involvement of the diesel fuel is significantly greater than for the gas phase spread over gasoline.

Nomenclature

A	Area (m^2)
A_s	Area of spill (m^2)
A_{ss}	Steady-state area of continuously flowing burning fuel spill (m^2)
C_p	Specific heat of liquid fuel
D	Diameter (m)
D_{ss}	Steady-state area of diameter of burning fuel spill (m)
DT	$T_{fl} - T_l$
Δh_c	Heat of combustion (kJ/kg)
$\Delta h_{v,sen}$	Sensible heat of vaporization (kJ/kg)
k	Extinction coefficient (m^{-1})
l	Length of a trench involved with fire (m)
l_{max}	Maximum length of trench (m)
L_f	Flame height (m)
$\dot{m}''$	Fuel-mass burning rate per unit area (kg/m^2s)
$\dot{m}''_\infty$	Fuel-mass burning rate per unit area for infinite size pools (kg/m^2s)
$\dot{m}''_{max}$	Maximum fuel-mass burning rate per unit area (kg/m^2s)
m_i	Mole fraction of fuel in liquid phase
n_i	Mole fraction of fuel in vapor phase
$\dot{Q}$	Heat release rate (kW)
r	Radius of the fire
$r_{A,max}$	Maximum radius of the fire for complete involvement of fuel release
t	Time
$t_{A,max}$	Time at which fuel release becomes completely involved
T_b	Boiling point temperature of liquid fuel
T_{fl}	Closed-cup flashpoint temperature of fuel
T_{gm}	Minimum liquid temperature at which asymptotic gas phase spread occurs
T_{go}	Liquid temperature at the transition from liquid to gas phase–controlled burning
T_l	Liquid fuel temperature
T_o	Initial temperature of liquid fuel
v	Flame spread velocity (cm/s)
V	Volume (m^3)
$\dot{V}_L$	Volumetric flow rate of liquid fuel (m^3/s)
w	Width of a trench (m)
$\dot{y}$	Regression rate (m/s)
$\dot{y}_{max}$	Maximum regression rate (m/s)

Greek Letters

β Mean-beam-length correction
ρ Density (kg/m^3)
δ Pool or spill depth (m)

References

1. C. Beyler, "Fire Hazard Calculations for Large Open Hydrocarbon Fires," *The SFPE Handbook of Fire Protection Engineering,* 4th ed., Springer (2015).
2. G.D. Chambers, "Flight Line Extinguisher Evaluation," U.S. Air Force Report DOD-AGFSRS-76-9 (1977).
3. D.T. Gottuk et al., Hughes Associates Inc., Internal Research, 2000.
4. D.T. Gottuk, J.L. Scheffey, F.W. Williams, J.E. Gott, and R.J. Tabet, "Optical Fire Detection (OFD) for Military Aircraft Hangars: Final Report on OFD Performance to Fuel Spill Fires and Optical Stresses," *NRL/MR/6180-00-8457,* Naval Research Laboratory, Washington, DC (2000).
5. A.D. Putorti, Jr., J.A. McElroy, and D. Madrzykowski, "Flammable and Combustible Liquid Spill/Burn Patterns," *NIJ Report 604-00,* National Institute of Justice, Washington, DC (2001).
6. A.T. Modak, "Ignitability of High-Fire-Point Liquid Spills," *EPRI NP-1731,* Factory Mutual Research Corporation, Norwood, MA (1981).
7. Benfer, M., "Spill and Burning Behavior of Flammable Liquids," Master's Thesis, University of Maryland, 2010.
8. Mealy, C.L., Benfer, M., and Gottuk, D.T., "Fire Dynamics and Forensic Analysis of Liquid Fuel Fires," Grant No. 2008-DN-BX-K168, Office of Justice Programs, National Institute of Justice, Department of Justice, February 18, 2011. https://www.ncjrs.gov/pdffiles1/nij/grants/238704.pdf
9. H.E. Moran, J.C. Burnett, and J.T. Leonard, "Suppression of Fuel Evaporation by Aqueous Films of Fluorochemical Surfactant Solutions," *NRL Report 7247,* Naval Research Laboratory, Washington, DC (1971).
10. Coordinating Research Council, *Handbook of Aviation Fuel Properties,* Alpharetta, GA (1983).
11. T. Kinbara, *Bulletin of the Institute of Physics and Chemical Research (Japan),* 9, p. 561 (1932).
12. J.H. Burgoyne and A.F. Roberts, "The Spread of Flame across a Liquid Surface, II. Steady-State Conditions," *Proceedings of the Royal Society A,* 308, pp. 55–68 (1968).
13. A.F. Roberts, Ph.D. Thesis, University of London (1959).
14. K. Akita, "Some Problems of Flame Spread along a Liquid Surface," in *Proceedings of the 14th International Symposium on Combustion,* Combustion Institute, Pittsburgh, PA, pp. 1075–1081 (1973).
15. R. Mackinven, J.G. Hansel, and I. Glassman, "Influence of Laboratory Parameters on Flame Spread across Liquid Fuels," *Combustion Science and Technology,* 1, pp. 293–306 (1970).
16. K.E. Torrance, "Subsurface Flows Preceding Flame Spread over a Liquid Fuel," *Combustion Science and Technology,* 3, pp. 133–143 (1971).
17. K.E. Torrance and R.L. Mahajan, "Fire Spread over Liquid Fuels: Liquid Phase Parameters," in *Proceedings of the 15th International Symposium on Combustion,* Combustion Institute, Pittsburgh, PA, pp. 281–287 (1975).
18. W.W. Hillstrom, "Temperature Effects on Flame Spreading over Fuels," *Paper to Eastern Section,* Combustion Institute, Pittsburgh, PA (1975).
19. I. Glassman and F.L. Dryer, "Flame Spreading across Liquid Fuels," *Fire Safety Journal,* 3, pp. 123–128 (1980).
20. A. Nakakuki, "Flame Spread over Solid and Liquid Fuels," *Journal of Fire & Flammability,* 7, pp. 19–40 (1976).
21. K. Akita and O. Fujiwara, "Pulsating Flame Spread along the Surface of Liquid Fuels," *Combustion and Flame,* 17, pp. 268–269 (1971).
22. H. Ishida, "Flame Spread over Fuel-Soaked Ground," *Fire Safety Journal,* 10, pp. 163–171 (1986).
23. H. Ishida, "Flame Spread over Ground Soaked with Highly Volatile Liquid Fuel," *Fire Safety Journal,* 13, pp. 115–123 (1988).
24. W.A. Sirignano and I. Glassman, "Flame Spreading above Liquid Fuels: Surface-Tension-Driven Flows," *Combustion Science and Technology,* 1, pp. 307–312 (1970).
25. T. Hirano, T. Suzuki, I. Mashiko, and N. Tanabe, "Gas Movements in Front of Flames Propagating Across Methanol," *Combustion Science and Technology,* 22, pp. 83–91 (1980).
26. A. Ito, D. Masuda, and K. Saito, "A Study of Flame Spread over Alcohols Using Holographic Interferometry," *Combustion and Flame,* 83, pp. 375–389 (1991).
27. F. Miller and H. Ross, "Further Observations of Flame Spread over Laboratory-Scale Alcohol Pools," *Proceedings of the 24th International Symposium on Combustion,* Combustion Institute, Pittsburgh, PA, pp. 1703–1711 (1992).
28. W.A. Sirignano, "A Critical Discussion of Theories of Flame Spread across Solid and Liquid Fuels," *Combustion Science and Technology,* 6, pp. 95–105 (1972).
29. D.D. Cline and L.N. Koenig, "The Transient Growth of an Unconfined Pool Fire," *Fire Technology,* 19, 3, pp. 149–162 (1983).
30. D. White, C.L. Beyler, C. Fulper, and J. Leonard, "Flame Spread on Aviation Fuels," *Fire Safety Journal,* 28, pp. 1–31 (1997).

31. J.T. Leonard, C.R. Fulper, R. Darwin, G.G. Back, R.E. Burns, and R. Ouelette, "Fire Hazards of Mixed Fuels on the Flight Deck," *Naval Research Laboratory Memorandum Report 6975* (1992).
32. H.D. Ross, "Ignition of and Flame Spread Over Laboratory-Scale Pools of Pure Liquid Fuels," *Progress in Energy and Combustion Science,* 20, pp. 17–63 (1994).
33. I. Glassman and J. Hansel, "Some Thoughts and Experiments on Liquid Fuel Spreading, Steady Burning, and Ignitability in Quiescent Atmospheres," *Fire Research Abstracts and Reviews,* 10, 3, pp. 297–322 (1948).
34. J.P. Burelbach, M. Epstein, and M.G. Plys, "Brief Communication—Initiation of Flame Spreading on Shallow Subflash Fuel Layers," *Combustion and Flame,* 114, 1/2, pp. 280–282 (1998).
35. I. Liebmann, J. Corry, and H.E. Perlee, "Flame Propagation in Layered Methane-Air Systems," *Combustion Science and Technology,* 1, pp. 257–267 (1970).
36. C.C. Feng, S.H. Lam, and I. Glassman, "Flame Propagation through Layered Fuel-Air Mixtures," *Combustion Science and Technology,* 10, pp. 59–71 (1975).
37. H. Phillips, "Flame in a Buoyant Methane Layer," *Proceedings of the 10th International Symposium on Combustion,* Combustion Institute, Pittsburgh, PA, pp. 1277–1283 (1965).
38. Military Specification, "Turbine Fuel, Aviation, Grades JP-4, JP-5, and JP-5/JP-8 ST," *MIL-T-5624N* (1989).
39. Military Specification, "Turbine Fuel, Aviation, Grades JP-8," *MIL-T-83133B* (1988).
40. K. Takeno and T. Hirano, "Behavior of Combustible Liquid Soaked in Porous Beds During Flame Spread," in *Proceedings of the 22nd International Symposium on Combustion,* Combustion Institute, Pittsburgh, PA, pp. 1223–1230 (1988).
41. H. Ishida, "Initiation of Fire Growth on Fuel-Soaked Ground," *Fire Safety Journal,* 18, pp. 213–230 (1992).
42. V.I. Blinov and G.N. Khudiakov, "Diffusion Burning of Liquids," U.S. Army Translation, *NTIS No. AD296762* (1961).
43. H.C. Hottel, "Certain Laws Governing Diffusive Burning of Liquids," *Fire Research Abstracts and Reviews,* 1, p. 41 (1959).
44. D.S. Burgess, A. Strasser, and J. Grumer, "Diffusive Burning of Liquid Fuels in Open Trays," *Fire Research Abstracts and Reviews,* 3, p. 177, (1961).
45. D.S. Burgess, J. Grumer, and H.G. Wolfhard, "Burning Rates of Liquid Fuels in Large and Small Open Trays," *International Symposium on the Use of Models in Fire Research, Publication 786,* National Academy of Sciences—National Research Council, Washington, DC, pp. 68–75 (1961).
46. M.G. Zabetakis and D.S. Burgess, "Research on Hazards Associated with the Production of and Handling of Liquid Hydrogen," *RI 5705,* U.S. Bureau of Mines (1961).
47. K.S. Mudan, "Thermal Radiation Hazards from Hydrocarbon Pool Fires," *Progress in Energy Combustion Science,* 10, pp. 59–80 (1984).
48. J. Grumer, A. Strasser, T.A. Kubala, and D.S. Burgess, "Uncontrolled Diffusive Burning of Some New Liquid Propellants," *Fire Research Abstracts and Reviews,* 3, p. 159 (1961).
49. V. Babrauskas, "Estimating Large Pool Fire Burning Rates," *Fire Technology,* 19, p. 251 (1983).
50. V. Babrauskas, "Heat Release Rates," in *The SFPE Handbook of Fire Protection Engineering,* 5th ed., Springer (2015).
51. J.A. Mansfield and L.J. Linley, "Measurement and Statistical Analysis of Flame Temperatures from Large Fuel Spill Fires," *NWC TP 7061,* Naval Weapons Center, China Lake, CA (1991).
52. Mealy, C.L. and Gottuk, D.T., "Ignitable Liquid Fuel Fires in Buildings – A Study of Fire Dynamics," Grant No. 2009-DN-BX-K232, Office of Justice Programs, National Institute of Justice, Department of Justice, January 31, 2013.
53. D.S. Burgess and M. Hertzberg, "Radiation from Pool Flames," *Heat Transfer in Flames,* Chapter 27 (N.H. Afgan and J.M. Beer, eds.), Scripta Book Co., Washington, DC (1974).
54. H.W. Emmons, "Some Observations on Pool Burning," *The Use of Models in Fire Research,* Publication 786 NAS-NRC, Washington, DC, pp. 50–67 (1961).
55. G. Heskestad, "Luminous Heights and Turbulent Diffusion Flames," *Fire Safety Journal,* 5, pp. 103–108 (1983).
56. A.M. Kanury, "Ignition of Liquid Fuels," *SFPE Handbook of Fire Protection Engineering,* National Fire Protection Association, Quincy, MA, pp. 2-188–2-199 (2002).
57. NFPA 325, *Guide to Fire Hazard Properties of Flammable Liquids, Gases, and Volatile Solids,* National Fire Protection Association, Quincy, MA (1994).

D.T. Gottuk is VP of Specialty Services and the Technical Director of Jensen Hughes. He is actively involved in fire hazard analyses, fire research and testing, and forensic engineering relative to fire dynamics and fire detection.

D.A. White is a Vice President at Jensen Hughes. His technical expertise is primarily focused in industrial fire protection, litigation services, and special hazards.